OPTICALLY PUMPED LASER

Annual Technical Report

October 15, 1976

For period covering
August 15, 1975 To August 15, 1976

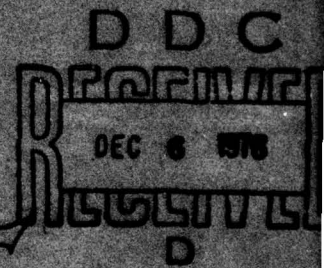Sponsored By

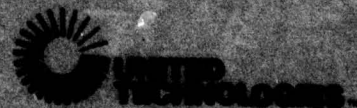Advanced Research Projects Agency

ARPA Order No. 1807

Contract No. N00014-74-C-0376

R.T. Brown

D D C

DEC 6 1976

UNITED TECHNOLOGIES
RESEARCH CENTER

EAST HARTFORD, CONNECTICUT 06108

REPORT DOCUMENTATION PAGE	READ INSTRUCTIONS BEFORE COMPLETING FORM

1. REPORT NUMBER R76-921853-12	2. GOVT ACCESSION NO.	3. RECIPIENT'S CATALOG NUMBER

Final technical rept.

4. TITLE (and Subtitle) OPTICALLY PUMPED LASER	5. TYPE OF REPORT & PERIOD COVERED Final Tech. 8/15/75 - 8/15/76
	6. PERFORMING ORG. REPORT NUMBER R76-921853-12

15 Aug 75 - 15 Aug 76

7. AUTHOR(s) Robert T. Brown	8. CONTRACT OR GRANT NUMBER(s) N00014-74-C-0376 ARPA order-1807

9. PERFORMING ORGANIZATION NAME AND ADDRESS United Technologies Research Center 400 Main Street East Hartford, CT 06108	10. PROGRAM ELEMENT, PROJECT, TASK AREA & WORK UNIT NUMBERS ARPA 72 p.

11. CONTROLLING OFFICE NAME AND ADDRESS Office of Naval Research Department of Navy Arlington, VA 22217	12. REPORT DATE 10/15/76
15 Oct 76	13. NUMBER OF PAGES

14. MONITORING AGENCY NAME & ADDRESS(if different from Controlling Office) Director, Physics Programs Physical Sciences Division Office of Naval Research 800 North Quincy St., Arlington, VA 22217	15. SECURITY CLASS. (of this report) Unclassified
	15a. DECLASSIFICATION/DOWNGRADING SCHEDULE

16. DISTRIBUTION STATEMENT (of this Report)

> **DISTRIBUTION STATEMENT A**
> Approved for public release;
> Distribution Unlimited

17. DISTRIBUTION STATEMENT (of the abstract entered in Block 20, if different from Report)

18. SUPPLEMENTARY NOTES

19. KEY WORDS (Continue on reverse side if necessary and identify by block number)

Optically-pumped electric-discharge laser
uv laser

20. ABSTRACT (Continue on reverse side if necessary and identify by block number)

This report describes experimental and theoretical studies of a new technique for pumping high-pressure electric-discharge lasers. Various coupling geometries were examined and studies were made of the discharge temporal evolution and coupling efficiency. Diffuse discharges were obtained at pressures up to 20 atm in an optical configuration which allowed the incorporation of a uv optical cavity and which coupled over 95% of the 10.6 micrometers radiation into the discharge. Studies of various kinetic systems were carried over

409252

out including He/N_2 at 337.1 nm, He/N_2 at 427.8 nm, $Xe/F_2/He$ at 354 nm, and $Kr/F_2/He$ at 249 nm.

UNITED TECHNOLOGIES RESEARCH CENTER

East Hartford, Connecticut 06108

Report Number: R76-921853-12
Final Technical Report for the period
15 August 1975 to 15 August 1976

OPTICALLY PUMPED LASER

ARPA Order No.:   1807
Program Code: 4E90K21
Contractor: United Technologies Research Center
Effective Date of Contract: 1 March 1974
Contract Expiration Date: 15 October 1976
Amount of Contract: $285,043
Contract Number: N00014-74-C-0376
Principal Investigator: Dr. David C. Smith (203) 565-5281
Scientific Officer: Director, Physics Programs
                                    Physical Sciences Division
                                    Office of Naval Research
                                    Department of the Navy
                                    800 North Quincy Street
                                    Arlington, VA   22217
Short Title: Optically Pumped Lasers
Report by: R. T. Brown

DDC
RECEIVED
DEC 6 1976
D
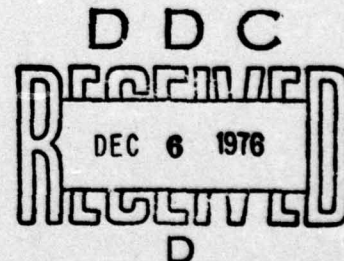
The views and conclusions contained in this document are those of the author
and should not be interpreted as necessarily representing the official
policies, either expressed or implied, of the Advanced Research Projects
Agency or the U. S. Government.

UNITED
TECHNOLOGIES

1

R76-921853-12

Optically Pumped Laser

TABLE OF CONTENTS

TABLE OF CONTENTS (Cont'd)

SECTION 1

TECHNICAL REPORT SUMMARY

Under this contract, a new technique for pumping high-pressure electric-discharge laser media was investigated. The objective of this program has been to develop high-energy, high-efficiency lasers operating in the ultraviolet and visible portions of the spectrum.

The basic elements of the optically-pumped electric discharge laser (OPEDL) concept have been described previously (Br75-1, Br74). The output laser pulse from a CO_2 TEA laser is focused into the active uv laser medium, which has been preionized to some low level of electron density. The 10.6 μ optical field then heats the electrons via inverse bremsstrahlung, and the electron density grows in a cascade process. The properties of this discharge are well suited to pumping various uv and visible laser transitions.

During the course of this study, the work focused on two general areas. The first area emphasized the efficient coupling of the 10.6 μ radiation into the discharge and involved the study of the discharge pumping physics (in particular the ionization kinetics), and also involved the development of optical configurations, preionization techniques, and cell geometries for the purpose of efficient discharge heating. The second area involved the study of various kinetic systems (e.g., the krypton-fluoride system) under conditions corresponding to good optically pumped electric discharge (OPED) operation.

Within the first area of emphasis, the results were very promising and the developmental efforts were successful, with the following significant results being achieved during the contract period.

1. Large-volume, scalable, diffuse discharges were obtained at pressures up to 20 atm.

2. An optical pumping geometry was developed which allowed the incorporation of an effective uv/visible cavity, and which would be compatible with high-repetition-rate operation.

3. Measurements showed that under the above conditions, over 95 percent of the 10.6 μ energy was coupled into the discharge.

4. A detailed understanding of the discharge pumping and temporal evolution processes was obtained.

Within the second area of emphasis, the results were negative, in that no kinetic system was found which demonstrated efficient conversion from 10.6 μ radiation to uv/visible laser radiation. However, this appeared to result from a mismatch between the conditions achieved in the optically-pumped discharge and the conditions required for efficient laser excitation, rather than from any fundamental limitation of the concept. Within the second area of emphasis, the following signigicant results were achieved.

1. uv lasing was demonstrated with the 2nd positive system of molecular nitrogen (337.1 nm). The efficiency was low due to the inherent low efficiency of this system and to inefficient optical coupling. A theoretical model of the He/N_2 kinetics correctly predicted the behavior of the discharge, and showed qualitative agreement with the experiments.

2. Experiments with the helium/nitrogen charge transfer system demonstrated good discharges at 20 atm, but indicated that the electron temperature was too low for efficient pumping of the charge transfer reaction.

3. Experiments with XeF and KrF demonstrated diffuse, large volume discharges, at F_2 and Xe/Kr pressures comparable to those used with other excitation schemes, but indicated that electron quenching prevented efficient population of the upper laser level.

Section 2 of this report gives a general outline of the approach used in these studies, and includes a description of the experiment.

Section 3 is a general summary of results obtained regarding discharge pumping effects, and compares various pumping geometries, as well as examining the discharge temporal evolution and coupling efficiency.

Section 4 describes studies at 337.1 nm in helium/nitrogen mixtures and is an extension of some of the work reported in Ref. (Br75-1).

Section 5 is a study of the He/N_2 charge-transfer system with OPED pumping.

Section 6 describes results obtained in $He/Xe/F_2$ mixtures and $He/Kr/F_2$ mixtures and shows that the spectra from the optically-pumped discharges in these gases are very similar to those obtained with e-beam excitation.

Section 7 is a summary of the results and gives recommendations for areas of further study.

SECTION 2

INTRODUCTION

There is a continuing interest in generating high power laser radiation in
the uv/visible portion of the spectrum. Recent advances with electrically excited
systems (BE75-1, E375, BBA76, BPD76, and CCLC) have opened up the possibility of
developing uv/visible lasers with overall efficiencies of 10-20 percent, and with
the potential for scaling to high average powers. Most of these studies have
utilized electron beams or fast electrical circuits to drive the discharge. Under
the present contract, a new technique for pumping high-pressure electric-discharge
laser media has been investigated. The objective of this program has been to
develop high-energy, high-efficiency lasers operating in the ultraviolet and
visible portions of the spectrum.

The basic elements of the optically-pumped electric discharge laser (OPEDL)
concept have been described previously (Br75-1, Br74). By way of review, the out-
put pulse from a CO_2 TEA laser (Fig. 2.1) is focused into the active uv laser
medium, which has been preionized to some low level of electron density. In the
present studies, the preionization was produced via photoionization from small
arcs in the uv laser medium. The 10.6 μ optical field then heats the electrons
via inverse bremsstrahlung, and the electron density grows in a cascade process.
The size of the discharge produced is determined by the size of the 10.6 μ laser
focal volume and by the size of the region illuminated by the preionizing radiation.
The properties of this discharge are such that it is well suited for pumping
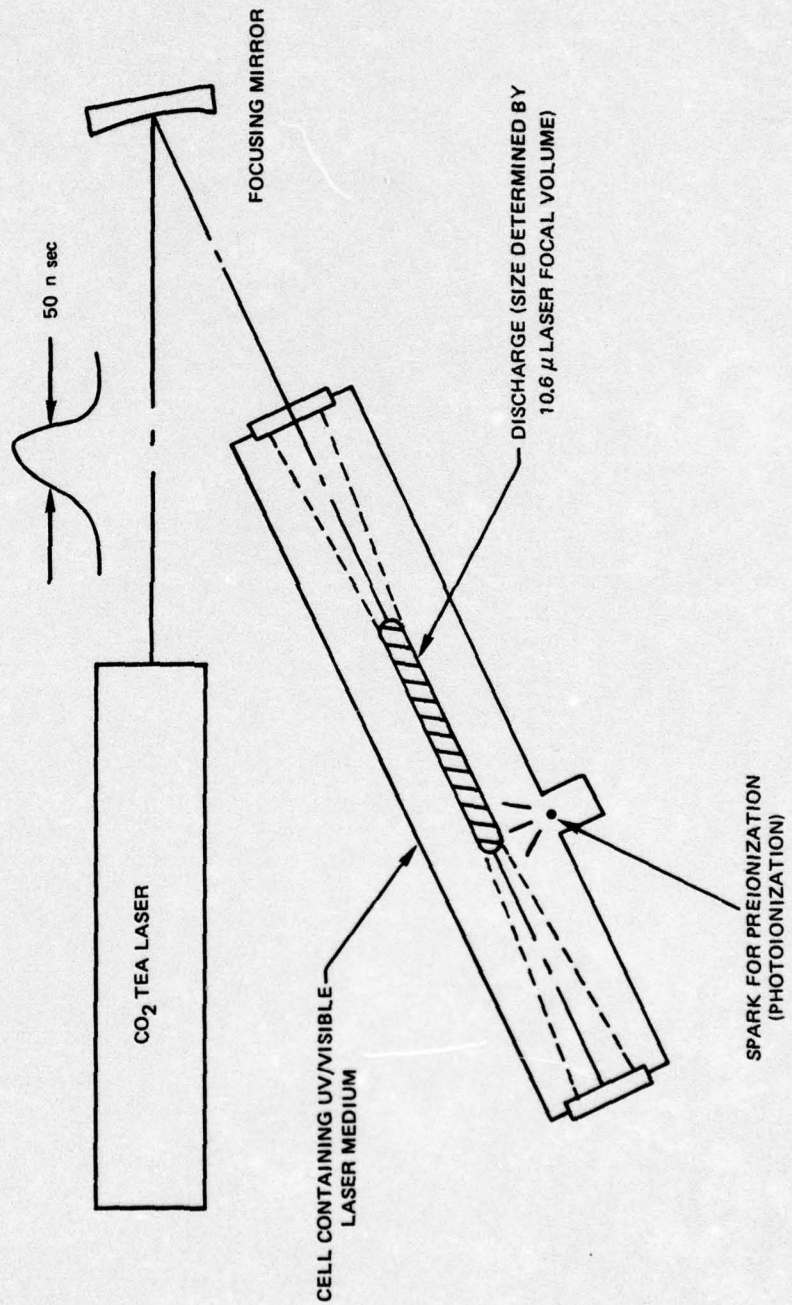various electronic transitions.

The present program has been primarily experimental in nature, with emphasis
on studying configurations and kinetic systems with the potential for scalability
and high overall efficiency (energy stored in the driver of the pumping laser to
uv/visible laser energy out). This is somewhat in contrast to the approach taken
with other excitation techniques (e.g., electron beams) in which the emphasis has
been on the intrinsic efficiency (i.e., uv/visible laser energy out vs energy
deposited in the gas). As discussed in Ref. (Br75-1) there are two steps in
developing a working laser. The first step is to find a kinetic system which has
a high intrinsic efficiency. The second step is to develop a pumping scheme which
can maintain this value of intrinsic efficiency over the entire active volume,
during a significant fraction of the pumping pulse, and which can maintain this
value of intrinsic efficiency when scaled to large sizes and when operated at high
repetition rates.

3

As discussed in Ref. (Br75-1) the OPEDL technique is unique in its ability to generate large-volume, diffuse, high-density, fast-risetime (sub-nanosecond) discharges in gases at high pressure (e.g., up to 30 atm). Also, since the energy is coupled into the cell through a transparent window (e.g., germanium) rather than through a metal foil, the repitition rate capability is limited only by that of the pumping laser. As will be discussed in the present report, the transfer of energy from the 10.6 μ pumping radiation to the uv laser plasma is very efficient, as opposed to the somewhat inefficient conversion from electron beam energy to useful energy deposited in the gas. For these reasons the OPEDL is attractive as a laser medium provided a kinetic system can be found whose pumping requirements are consistent with the properties inherent in the optically-pumped discharge.
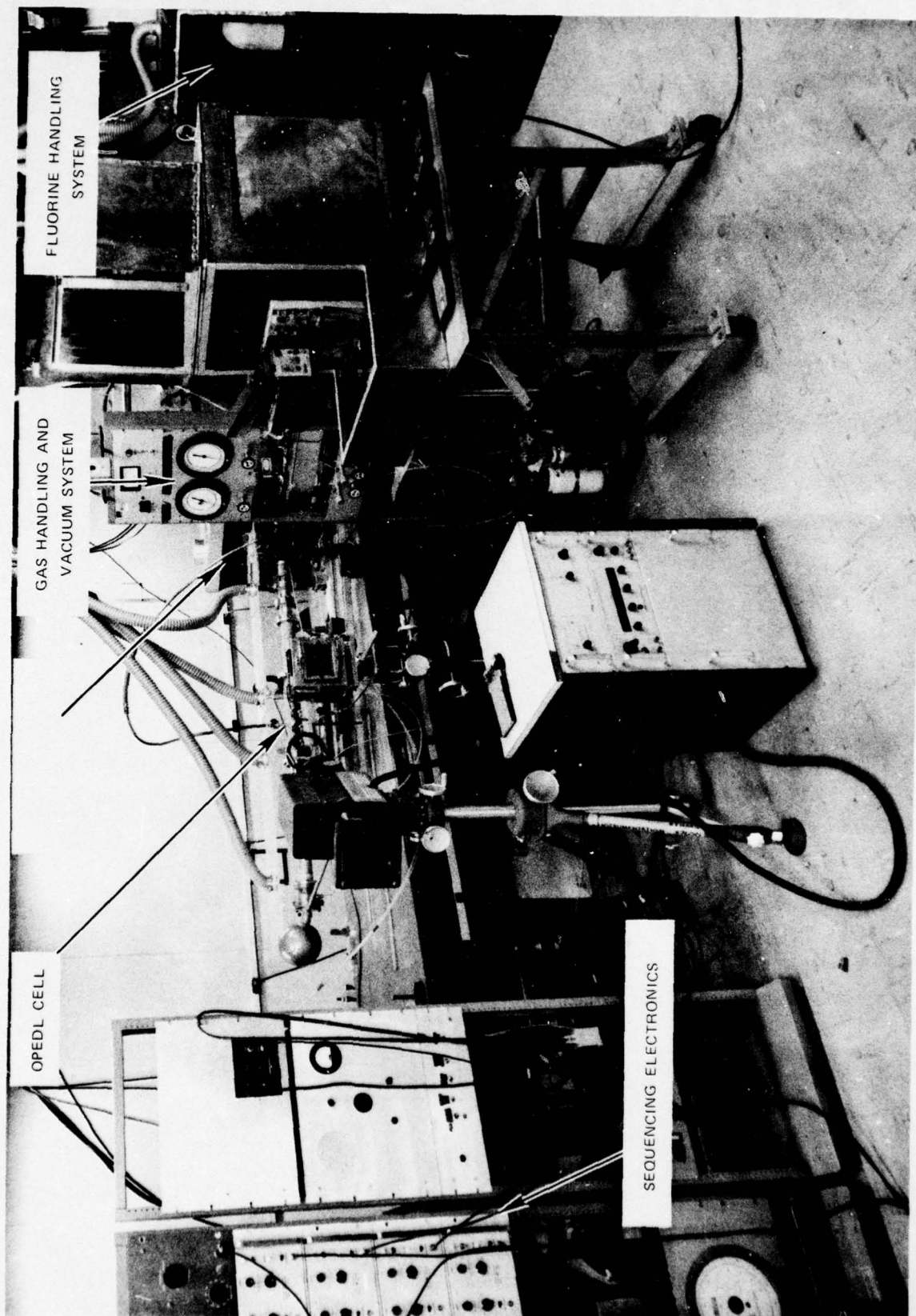
Because the optically-pumped discharge operates as a self sustained discharge, and because the desired transitions originate from electronic levels, the pumping kinetics (i.e., formation of the upper laser level) and the ionization kinetics are coupled, making it impossible to vary one without varying the other. For this reason, emphasis was placed on investigating the discharge pumping physics and on developing pumping geometries which could by operated with practical uv laser cavities. These discharges were then studied for their applicability to some of the recently developed charge-transfer and rare-gas halide kinetic systems.

A photograph of the experimental arrangement is shown in Fig. 2.2. The pumping laser was a Lumonics TEA 601 A oscillator, whose operating and output characteristics were described in Ref. (Br75-1). When operated with a $CO_2/N_2/He$ mixture, the laser had a nominal output energy of 75 J, a peak power of 300 MW, and a gain-switched pulse shape consisting of a 100 nsec (halfwidth) spike, followed by a 1.5 μsec tail. During this reporting period, the cell and gas handling system were modified to allow the use of fluorine and other halogens. The diagnostics consisted of time integrated and time resolved spectral measurements of laser and fluorescence radiation from the discharges, of photographs of the discharges, and of chemical analyses of the working gas mixtures.

FIG. 2.1

OPTICALLY–PUMPED ELECTRIC DISCHARGE

FOCUSING MIRROR

50 n sec

CO_2 TEA LASER

DISCHARGE (SIZE DETERMINED BY
10.6 μ LASER FOCAL VOLUME)

CELL CONTAINING UV/VISIBLE
LASER MEDIUM

SPARK FOR PREIONIZATION
(PHOTOIONIZATION)

FIG. 2.2

OPTICALLY—PUMPED DISCHARGE EXPERIMENT

FLUORINE HANDLING SYSTEM

GAS HANDLING AND VACUUM SYSTEM

OPEDL CELL

SEQUENCING ELECTRONICS

SECTION 3

DISCHARGE PUMPING STUDIES

3.1 Introduction

As mentioned in Section 2, the pumping kinetics and the ionization kinetics
of the optically pumped discharge are coupled, and it was only possible, as well
as being desirable, to study the kinetics of a given system (e.g., krypton
fluoride) within the context of a given pumping configuration. During the course
of this program a number of studies were carried out to gain a better understanding
of the physics of the discharge pumping process as well as to demonstrate the
ability to efficiently couple the 10.6 μ radiation into the discharge and to couple
the uv radiation out. These studies were general in nature, and the results are
applicable to any of the kinetic systems studied.

3.2 Coupling Geometries

The earliest work with the OPEDL technique (BS74) utilized a TEM$_{oo}$ gaussian
beam with spherical focusing optics, and produced a high-aspect-ratio discharge.
With this geometry it was very difficult to place a uv cavity around the discharge
because of the need to keep the uv optical elements out of the focused region of
the 10.6 μ beam. The use of prisms, gratings, and dichroic reflectors, often used
in coaxially pumped dye lasers, were not deemed practical because of the high
intensities (10^8-10^9 W/cm^2 (Br75-1)), encountered here. It was therefore desirable
to look for other configurations.

The most direct approach to solving this problem is to pump transverse to the
uv optical axis, as is done with direct e-beam excitation, e-beam sustained
discharge excitation, blumlein discharge excitation and uv preionized discharge
excitation. Experiments were carried out using transverse optical pumping, and
the setup used for these studies is sketched in Fig. 3.1 along with some photos
of the discharges obtained. As discussed in Ref. (Br74), the discharges were
dominated by hot spots, apparently due to nonuniformities in the transverse profile
of the 10.6 μ laser. Because of these problems, and because of the success with
other geometries, no further studies were carried out with transverse pumping.

A second geometry which was tried involved the use of an axicon mirror and a
spherical focusing lens/mirror as shown in Fig. 3.2. (See Ref. (Br74)). A typical
discharge obtained with this arrangement is also shown in Fig. 3.2. These discharges
tended to have a very high aspect ratio, and showed a lack of uniformity along the
axis which reflected the variation in the 10.6 μ intensity along the axis.

A third geometry which was used is shown in Fig. 3.3. This arrangement consisted of operating the TEA laser in an unstable resonator configuration and focusing the beam with a very long focal length mirror. Using such an arrangement, discharges up to 65 cm in length were obtained, as shown in Fig. 3.3. With this arrangement, various uv laser experiments were carried out, as described in Ref. (Br75-1) and in Section 4 below. These experiments required a very high aspect ratio cell in order to allow placing the input window well away from the focal region of the 10.6 μ beam.

The most practical arrangement developed in these studies was that shown in Fig. 3.4. With this arrangement, the CO_2 TEA laser was operated with a 200 m radius total reflector, and a flat, 65 percent reflecting output coupler. It was found that this gave a 10.6 μ beam with a very uniform transverse profile and with a divergence (full angle) of 7 mrad. When focused with a relatively short focal length spherical mirror, this arrangement then gave a very diffuse and uniform (based on time-integrated photographs) discharge with a length of 25-30 cm and a diameter of 1 cm, as shown in Fig. 3.4.

3.3 Discharge Scaling

As mentioned previously, a major consideration with any pumping technique is its scalability. Some pumping approaches (e.g., the blumlein discharge and the coaxial flashlamp) rely on certain properties (e.g., low inductance) for their effectiveness, and their efficiency falls off if they are scaled beyond a certain size. By way of contrast, a large number of data were obtained which indicated that the optical pumping approach is truly a volumetric process, and that the size of the discharge is determined by the size of the 10.6 μ laser focal volume, as shown in Fig. 3.5. This figure shows the discharges obtained for a variety of values for the 10.6 μ focusing mirror focal length F, the 10.6 μ laser divergence θ and the nominal focal diameter d.

3.4 Temporal Evolution

Since the multi-mode beam configuration shown in Fig. 3.4 appeared to be the most suitable for applications of the OPEDL technique, a rather detailed study was made of the coupling physics for this configuration. It was observed that the most uniform and symmetrical discharges were obtained with a single preionizing spark located just beyond the focus as shown schematically in Fig. 3.6. It appeared that the discharge evolved as a segment of plasma which swept from the preionization region back toward the laser, as indicated in Fig. 3.6.

While detailed modeling calculations of this process were not carried out, a qualitative explanation of this process can be obtained by looking at the inverse bremsstrahlung absorption length ℓ_a, given by the expression

$$\ell_a = \frac{m_e \epsilon_o c(\omega^2 + \nu^2)}{[e]\, e^2\, \nu} \quad , \tag{3.1}$$

where m_e is the electron mass, ϵ_o is the free-space permittivity, c is the speed of light, ω is the laser angular frequency, [e] is the electron density, and ν is the electron-heavy particle momentum transfer collision frequency. For a given gas mixture and pressure, ν is fixed, and ℓ_a varies inversely with the electron density. Thus, as the 10.6 μ intensity increases during the pumping pulse, the absorption length decreases as the electron density increases, decreasing fastest near the focus. At some point the absorption length becomes short compared to the focal volume length, and the plasma shields points beyond the focus. As the 10.6 μ intensity continues to increase during the pulse, the region of maximum absorption (i.e., highest 10.6 μ intensity) sweeps toward the laser, as shown in Fig. 3.6. For a discharge in helium at 17 atm, and an electron temperature of 2 eV, an absorption length of 1 cm corresponds to an electron density of 1.4×10^{16} cm^{-3}.

Several measurements were carried out which verified the above picture. The first consisted of monitoring the side fluorescence at a given point along the discharge for various values of the peak 10.6 μ intensity $I_{10.6})_o$. It was found that the peak fluorescence signal was insensitive to $I_{10.6})_o$ but that increasing $I_{10.6})_o$ resulted in the plasma moving further back toward the laser (as observed in time-integrated photographs).

A second measurement was carried out as shown in Fig. 3.7. The side fluorescence at 337.1 nm was observed at two points along the cell. As seen from the traces, the plasma segment had a characteristic length of $\lesssim 6$ cm, and swept past the windows with a velocity of $\sim 3 \times 10^8$ cm/sec. It should be noted that the fluorescence behind the plasma segment decays in ~ 40 nsec. This is much faster than the recombination time, and implies that, as indicated in Fig. 3.6, the electron temperature behind the plasma front decays very quickly.

This mode of evolution of the discharge has several implications regarding the use of the optically pumped discharge as a laser medium. The effect of the discharge evolution will depend on whether the uv laser is operated as an oscillator or as an amplifier, and whether or not the excited state lifetime is long compared to the discharge evolution time. If the excited state lifetime is long, then the effect of the discharge evolution can be ignored, and the effective gain length is the time-integrated discharge length. If the excited state lifetime is short, then the effective gain length is comparable to the plasma segment length, and the gain region will move along the axis during the pumping pulse. This mode of

operation should be acceptable, provided that the gain length is long enough to reach the oscillation threshold, or to provide a reasonable total gain, in the case of an amplifier, and provide that the high [e], low $\bar{u}_e$ region does not introduce loss processes at the uv laser wavelength.

3.5 Coupling Efficiency

A major concern with the OPEDL approach is that the electron density starts at a low value and cascades to a value at which the absorption of the 10.6 μ radiation is effective. In earlier studies (Br75-2), in which the spatial evolution effects described above were not considered, the total calculated efficiency was reduced considerably by the low absorptivity of the plasma during the initial portion of the pumping pulse. As mentioned above, with the configuration shown in Figs. 3.4 and 3.6, the plasma evolves in such a way that the time integrated absorption can be very large. This effect was verified experimentally by measuring the transmitted 10.6 μ pulse shape with a gold-doped germanium detector, and the results are shown in Fig. 3.8. It can be seen that for these conditions, over 95 percent of the incident 10.6 μ energy was absorbed by the plasma.

3.6 Incorporation of a uv Optical Cavity

One of the major efforts under this contract has been to develop a pumping configuration which would provide efficient coupling between the 10.6 μ radiation and the discharge, and at the same time allow the incorporation of an effective uv optical cavity. Such a configuration is shown in Fig. 3.9. With this setup, the 10.6 μ beam was clipped slightly to minimize reflections back toward the TEA laser. The total uv reflector was mounted internal to the cell as shown, and a cone shaped aperture was used at the far end of the cell to avoid reflections of the 10.6 μ radiation back on to the uv mirror. The uv output coupler was typically mounted external to the cell, with a quartz window used to seal the cell as shown. This arrangement held up well under hundreds of shots at high 10.6 μ flux levels, could be conveniently operated at pressures up to 20 atm, and was compatible with the use of corrosive gases such as F_2. It can be seen that this configuration is scalable by increasing the diameter of the 10.6 μ beam and increasing the focal length of the focusing mirror, and that the geometry is compatible with transverse gas flow for high-rep-rate operation.
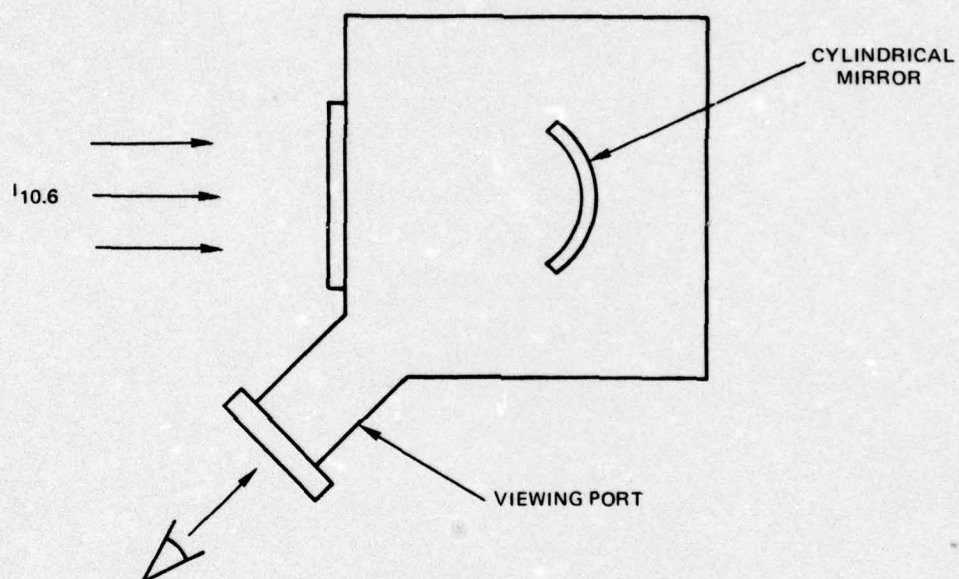
3.7 Conclusions Regarding Discharge Pumping

As outlined above, a system design was developed which allowed the efficient coupling of 10.6 μ pump radiation into a diffuse discharge. This efficient coupling

requires that the discharge operate in a regime where the absorption length is short compared to the focal volume length. Also, the 10.6 μ peak intensity (determined by the total 10.6 μ power and the focal diameter) must be high enough for the absorption length (through its dependence on [e]) to reach a value small compared to the focal volume length, early in the pumping pulse. For the conditions of Fig. 3.7 and using an absorption length of 5.0 cm (based on the pulse overlap in Fig. 3.7-b), the peak electron density is estimated to be $[e]_{max} \approx 3 \times 10^{15}$ cm^{-3}. This is a very high electron density for discharge excitation and, as will be discussed in Section 6, may lead to adverse quenching effects.

Looking at Eq. (3.1), we see that for a given value of ℓ_a, the minimum value of [e] corresponds to the conditions $\nu = \omega$. For 10.6 μ radiation, for an absorption length ℓ_a = 20 cm, and for $\nu = \omega$ (i.e., for a large system operating at very high pressures), we obtain $[e]_{min}$ = 3 x 10^{14} cm^{-3}. This value of electron density would be more compatible with systems such as krypton-fluoride.
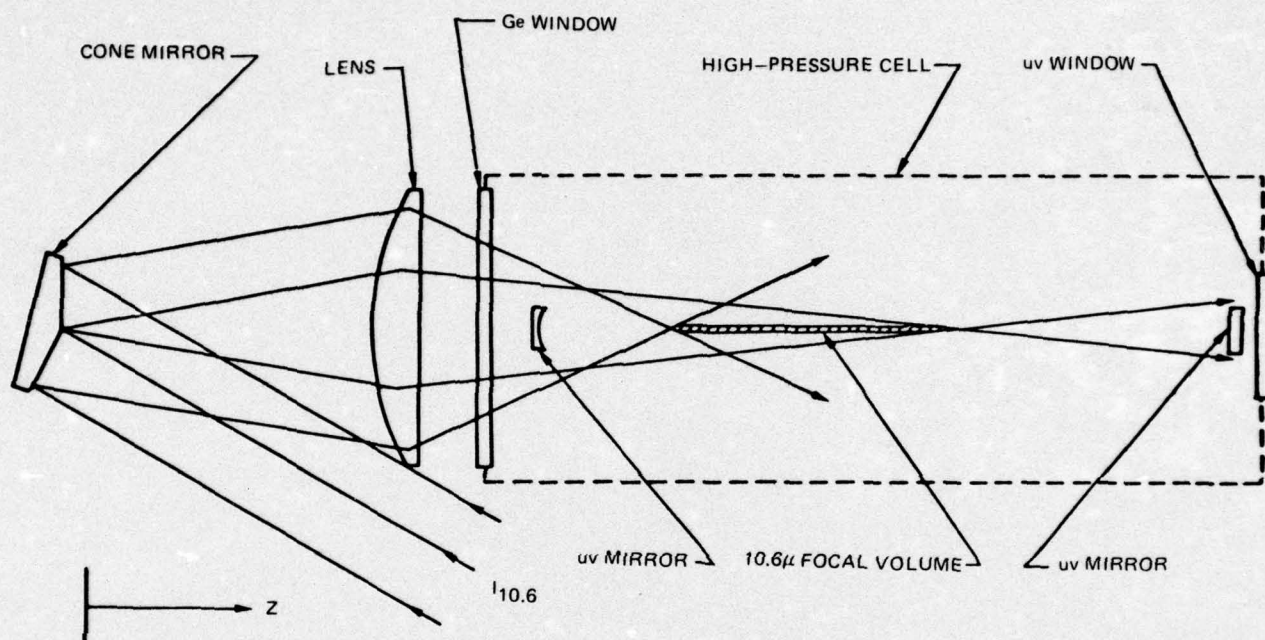
FIG. 3.1

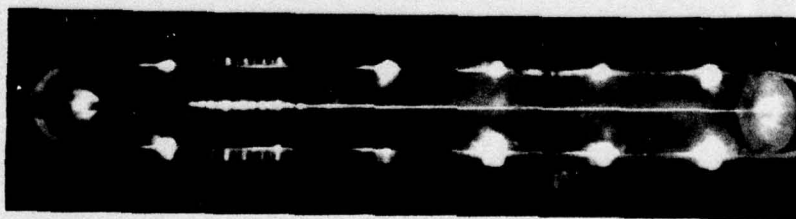**TRANSVERSE FOCUSING**

(a) DIAGRAM OF VIEWING ARRANGEMENT

(b) DISCHARGE PHOTOGRAPHS

AXICON FOCUSING

CONE MIRROR

LENS

Ge WINDOW

HIGH–PRESSURE CELL

uv WINDOW

Z

I$_{10.6}$
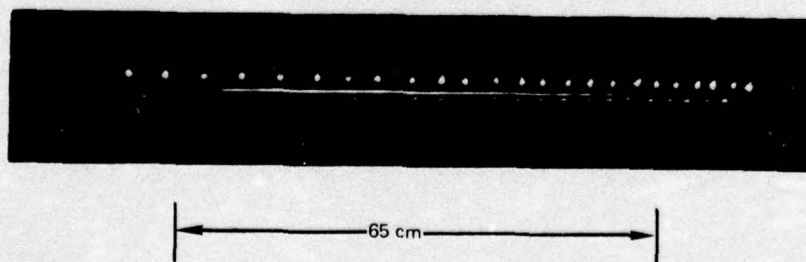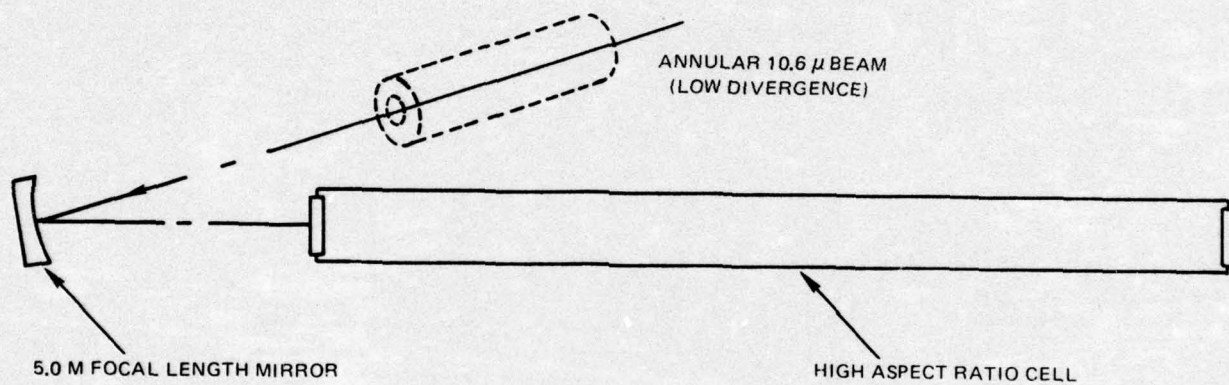
uv MIRROR

10.6μ FOCAL VOLUME

uv MIRROR

(a) DIAGRAM OF OPTICAL GEOMETRY

(b) PHOTO OF DISCHARGE–HELIUM AT 1 atm

FIG. 3.3

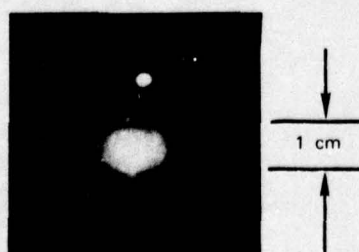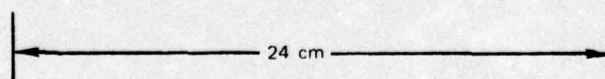## UNSTABLE RESONATOR BEAM WITH COAXIAL FOCUSING

ANNULAR 10.6 μ BEAM
(LOW DIVERGENCE)

5.0 M FOCAL LENGTH MIRROR

HIGH ASPECT RATIO CELL

65 cm

76—09—194—2

FIG. 3.4

MULTI—MODE BEAM WITH COAXIAL FOCUSING

UNIFORM 10.6 μ BEAM
(HIGH DIVERGENCE)

1.5 M FOCAL LENGTH MIRROR

LOW ASPECT RATIO CELL
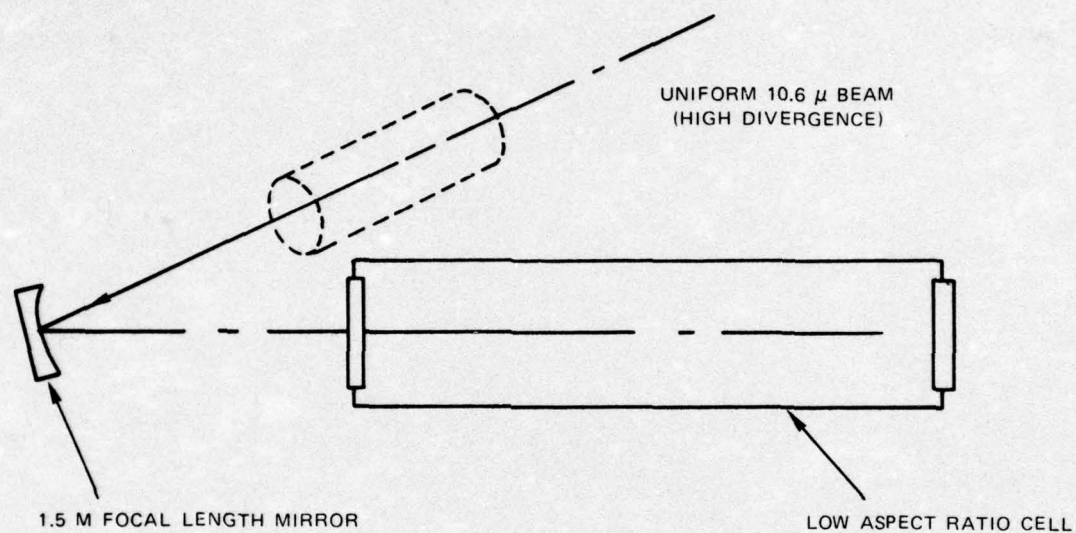
(a) SIDE VIEW OF
DISCHARGE

24 cm

(b) END VIEW OF DISCHARGE

1 cm

FIG. 3.5

DISCHARGE SCALING

(a)

F = 1.06 m

θ = 0.5 m RAD

d = 0.05 cm

←————13 cm————→

(b)

F = 5.0 m

θ = 0.5 m RAD

d = 0.25 cm

←————65 cm————→

(c)

F = 1.5 m

θ = 5 m RAD

d = 0.75 cm

←————30 cm————→

FIG. 3.6
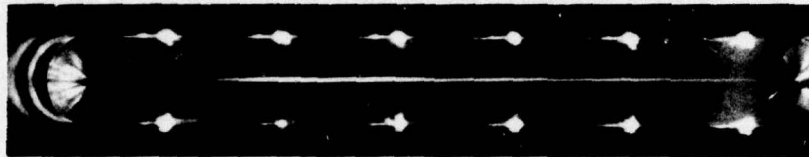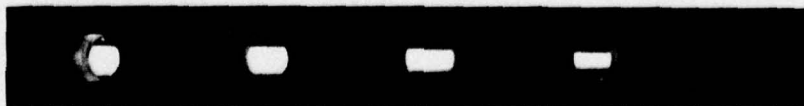
SCHEMATIC OF OPTICALLY—PUMPED DISCHARGE EVOLUTION

TEA LASER PULSE SHAPE

PREIONIZING SPARK

ℓ_a

PUMPING LASER FOCAL VOLUME

TIME

HIGH [e] LOW $\bar{u}_e$

HIGH [e] HIGH $\bar{u}_e$

FIG. 3.7
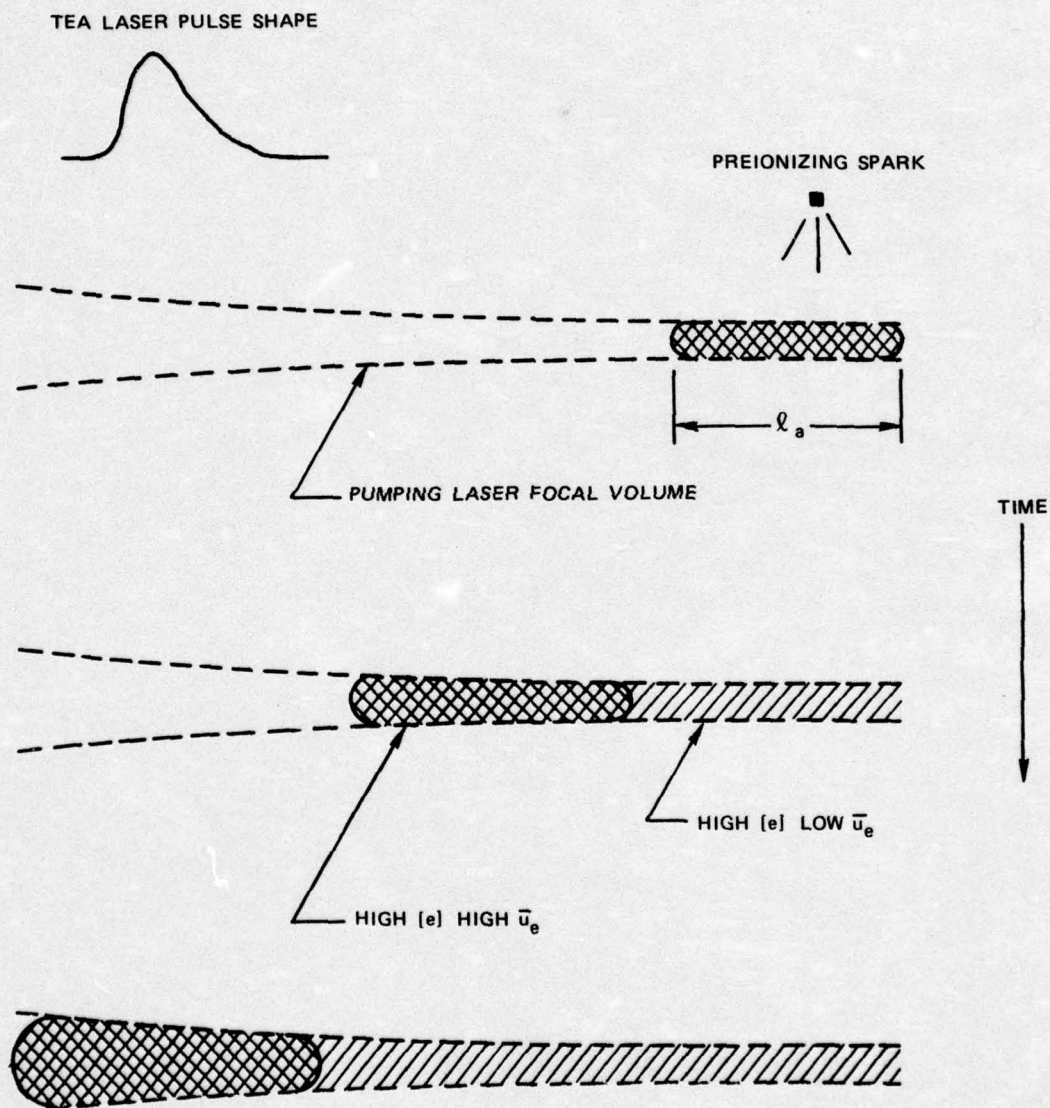
DISCHARGE EVOLUTION EXPERIMENT

(He/N_2 GAS MIXTURE)
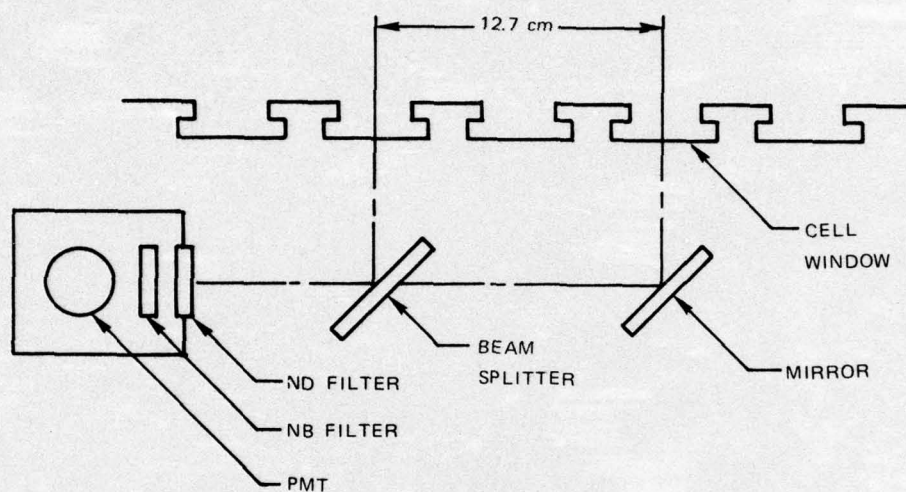
(a)

SCHEMATIC OF
DETECTOR
SETUP

CELL
WINDOW

BEAM
SPLITTER

MIRROR

ND FILTER

NB FILTER

PMT

12.7 cm
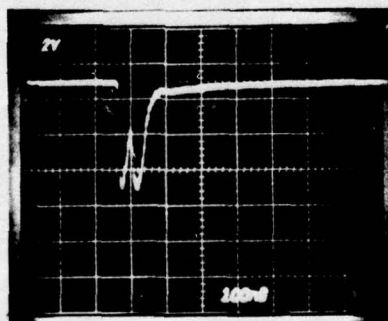
(b)

p_{N_2} = 20 TORR, p_{He} = 17 atm
BEAM SPLITTER IN PLACE
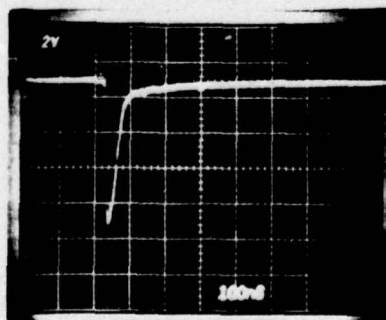
(c)

p_{N_2} = 20 torr, p_{He} = 17 atm
BEAM SPLITTER REMOVED

76-09-185-2

10.6μ ABSORPTION MEASUREMENT

$p_{F_2} = 1$ torr, $p_{Xe} = 10$ torr, $p_{He} = 17$ atm

(a) INCIDENT
10.6μ PULSE
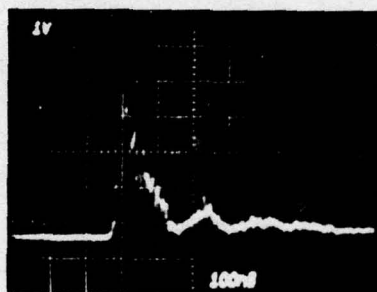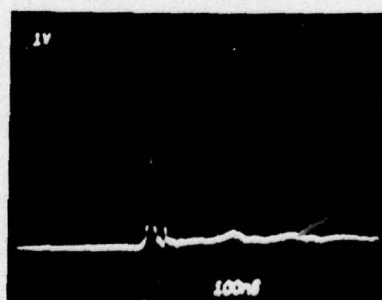
(b) TRANSMITTED
10.6μ PULSE

FIG. 3.9

CONFIGURATION USED IN RARE–GAS HALIDE OPTICAL EXTRACTION STUDIES
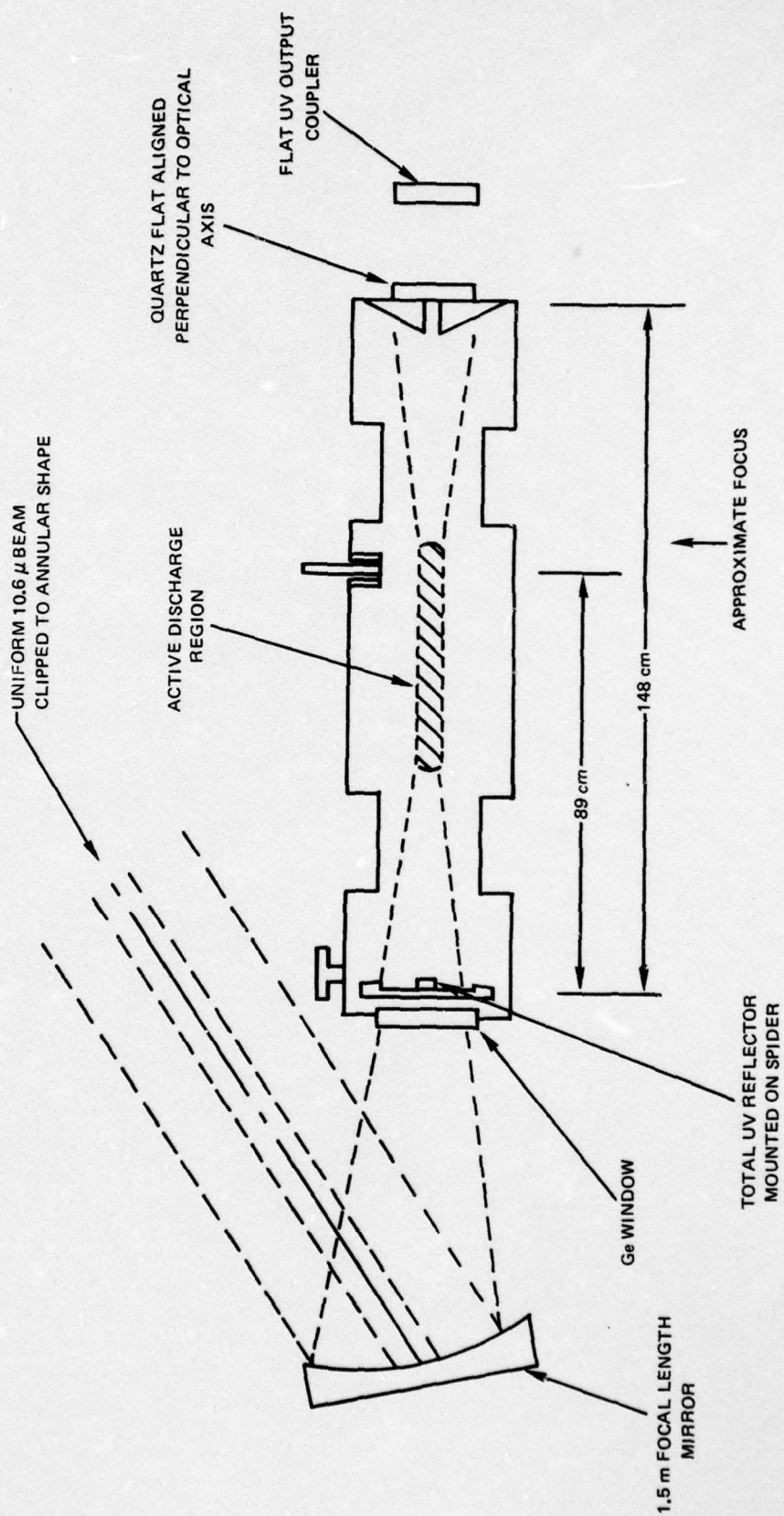
SECTION 4

STUDIES AT 337.1   IN HELIUM/NITROGEN MIXTURES

4.1 Introduction

As discussed in Ref. (Br75-1) studies were carried out using the OPEDL operating on the second positive transitions in molecular nitrogen. Since the appropriate rates for this system were known, the kinetics could be modeled accurately and used to gain insight into the physics of the optically-pumped discharge.

4.2 Theoretical Studies

The coupled rate equations for the nitrogen second positive system were integrated numerically, starting with an initial electron density and with a given $10.6\ \mu$ pulse shape and amplitude. The results of this analysis were described in Ref. (Br75-1) and will not be discussed in detail here. For the purpose of comparing the nitrogen second positive system with other kinetic systems studied during this contract period, it is useful to examine the partial energy level diagram in Fig. 4.1. The lasing transitions are from the $C^3\pi_u(\nu=0)$ to the $B^3\pi_g(\nu=0,1)$ states at 337.1 nm and 357.7 nm respectively, with excitation via electron impact excitation. For the optimum value of electron average energy, approximately 10 percent of the electron energy loss is into the desired $C^3\pi_u$ state. If the electron energy is too low, losses to vibration and lower electronic levels dominate, and if the electron energy is too high, losses to ionization dominate. The optimum electron average energy $\overline{u}_e$ was calculated to be ~ 4 eV. It was shown in Ref. (Br75-1) that the requirement for $\overline{u}_e \sim 4$ eV leads to the need for very short (< 10 nsec) pumping pulses, and that the tradeoff between optimized pumping of the laser transition and optimized coupling of the pump energy into the discharge adds an additional limit to the efficiency. It was also shown that in order to maximize the efficiency, it was necessary to operate with a saturated uv optical field, and that, because of the short gain duration, this was most likely to occur operating in an amplified spontaneous emission mode, with a long gain length and with vary fast pumping.

4.3 Experimental Studies

Experiments were carried out using the geometry shown in Fig. 3.3, with a typical configuration being shown in Fig. 4.2. As discussed in Ref. (Br75-1) lasing was obtained on the $C^3\pi_u \rightarrow B^3\pi_g$ (0,0) and (0,1) transitions, under a variety of conditions. During the present reporting period, these studies were extended by

modifying the cell to accommodate a longer focal length 10.6 μ beam. The objectives of these tests were to demonstrate scaling, and to reach a saturated flux condition in the amplified spontaneous emission mode.

Photographs of typical discharges, obtained with a 5.0 m focal length mirror, are shown in Fig. 4.3. These discharges were approximately a factor of two larger in physical length than those reported previously (Br75-1). Using this arrangement, a number of laser tests were carried out to measure the amplified spontaneous emission from one end of the discharge. The peak power at 337.1 nm was ∼ 2 kW, with a total pulse energy of ∼ 0.03 mJ, corresponding to a conversion efficiency from 10.6 μ to 337.1 nm of 0.0003 percent. A photograph of the laser spot on a fluorescent screen is shown in Fig. 4.4, and indicates a beam divergence of ∼ 3 mRad. The uv pulse and the 10.6 μ pumping pulse are shown in Fig. 4.4. The 10.6 μ laser was self mode locked, and it can be seen that the 337.1 nm pulse followed the 10.6 μ pulse shape very closely. From Fig. 4.4 it can be seen that the uv transition was above threshold for only the three most intense 10.6 μ spikes, and this is a major factor contributing to the low conversion efficiency.

As discussed in Ref. (Br75-1) studies were carried out with a two-pass optical cavity in which a small mirror was mounted near the input end of the cell. Results obtained with this arrangement are shown in Fig. 4.5. It was shown in Ref. (Br75-1) that with the uv mirror, the central portion of the uv beam (∼ 2 mm dia) was enhanced considerably by passage back through the discharge region. For the measurements in Fig. 4.5, a 2 mm aperture was placed in front of the detector in order to look only at the portion of the beam enhanced by the uv mirror. It can be seen that the uv cavity gave approximately a factor of ten increase in peak intensity at 337.1 nm.

A limited number of experiments were also carried out using the geometry shown in Fig. 3.4. Tests were run both in the amplified spontaneous emission mode and with an optical cavity similar to that in Fig. 3.9. The pumping pulse shape was as shown in Fig. 3.8-a, and the N_2 fraction was varied over the range 0.01% - 1%. With this configuration, no evidence of lasing was observed indicating that the fast risetime of the self mode locked 10.6 μ pulse train, seen in Fig. 4.4-c, is necessary in order to overcome the quenching losses of this system.

The conclusions regarding the He/N_2 second positive OPEDL studies can be summarized as follows:

1) Large volume OPEDL discharges were obtained (65 cm in length),

2) uv lasing was obtained in the amplified spontaneous emission mode and with a two-pass optical cavity,

3) uv lasing required the fast 10.6 μ risetimes corresponding to the self-mode-locked TEA laser pulse, and

11

4) The conversion efficiency was very low, apparently due to inefficient
   uv optical coupling and to the dynamics of the pumping kinetics (Br75-1).

FIG. 4.1

PARTIAL ENERGY LEVEL DIAGRAM FOR He/N$_2$ SYSTEM

FIG. 4.2
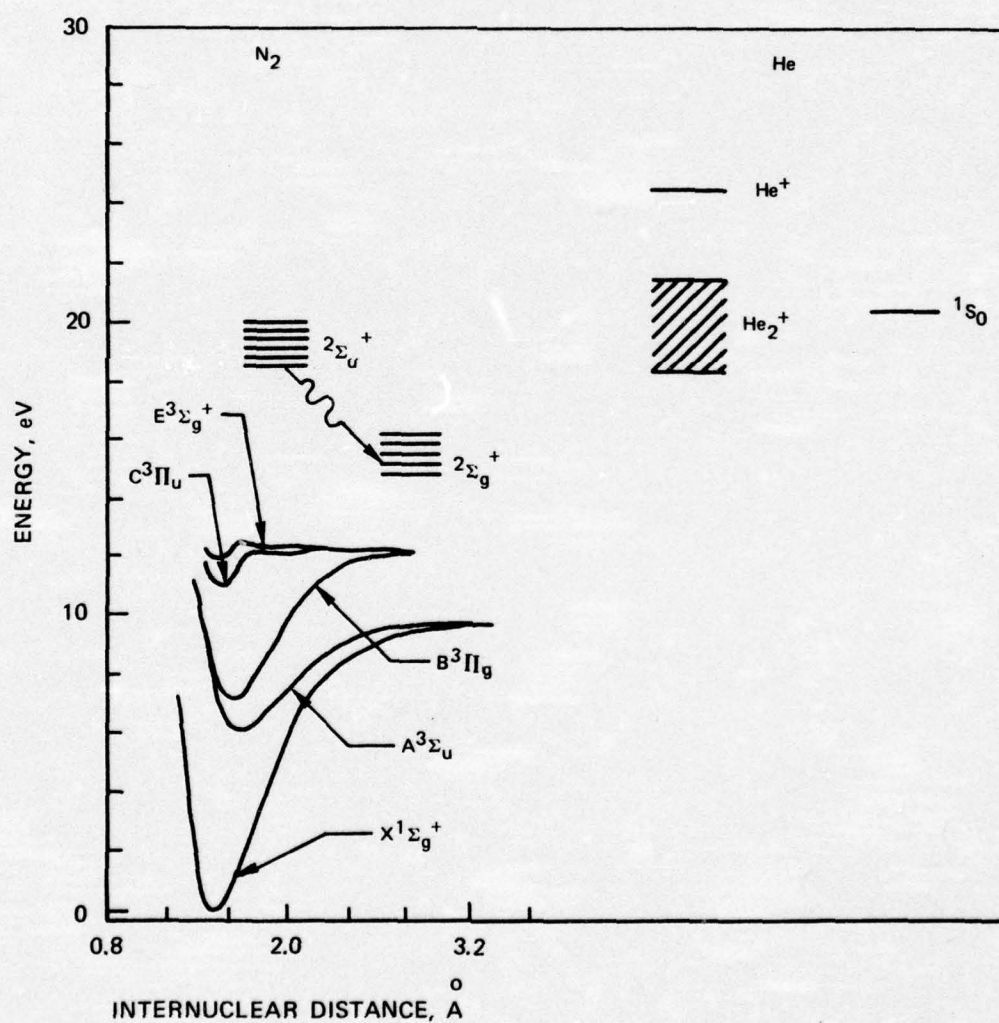
EXPERIMENTAL ARRANGEMENT USED IN COAXIAL STUDIES

LARGE TEA LASER IN UNSTABLE RESONATOR MODE

TEA LASER WITH UNSTABLE RESONATOR OPTICS

QUARTZ WINDOW

NEUTRAL DENSITY FILTERS

N.B. 3371Å FILTERS

PHOTODETECTOR

IRIS

2.7m FOCAL LENGTH MIRROR

Ge WINDOW

FIG. 4.3
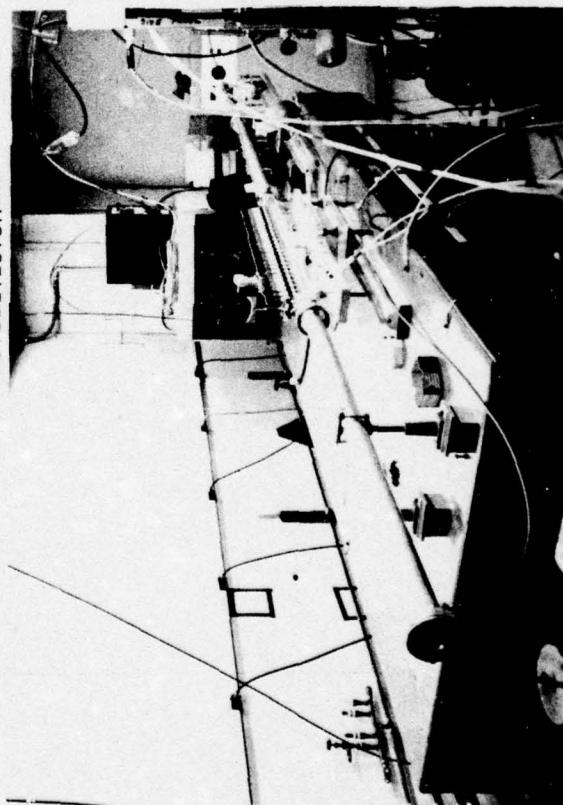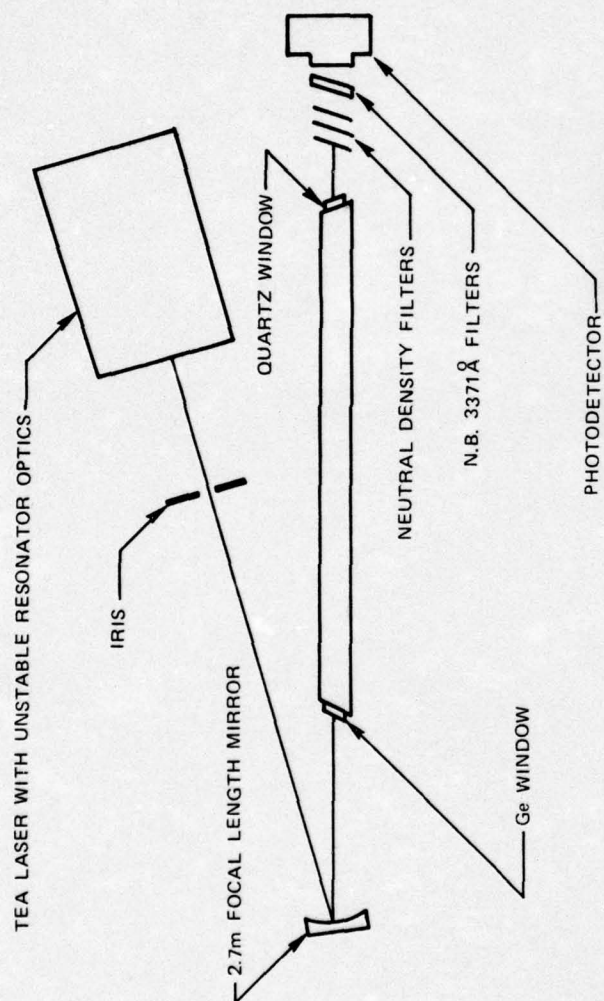
OPTICALLY PUMPED DISCHARGE

P = 1.0 atm X_{N_2} = 0.10 X_{He} = 0.90   5.0m FOCAL LENGTH MIRROR

a) 10.6μ PEAK INTENSITY JUST BELOW BREAKDOWN THRESHOLD

b) 10.6μ PEAK INTENSITY JUST ABOVE BREAKDOWN THRESHOLD

65 cm
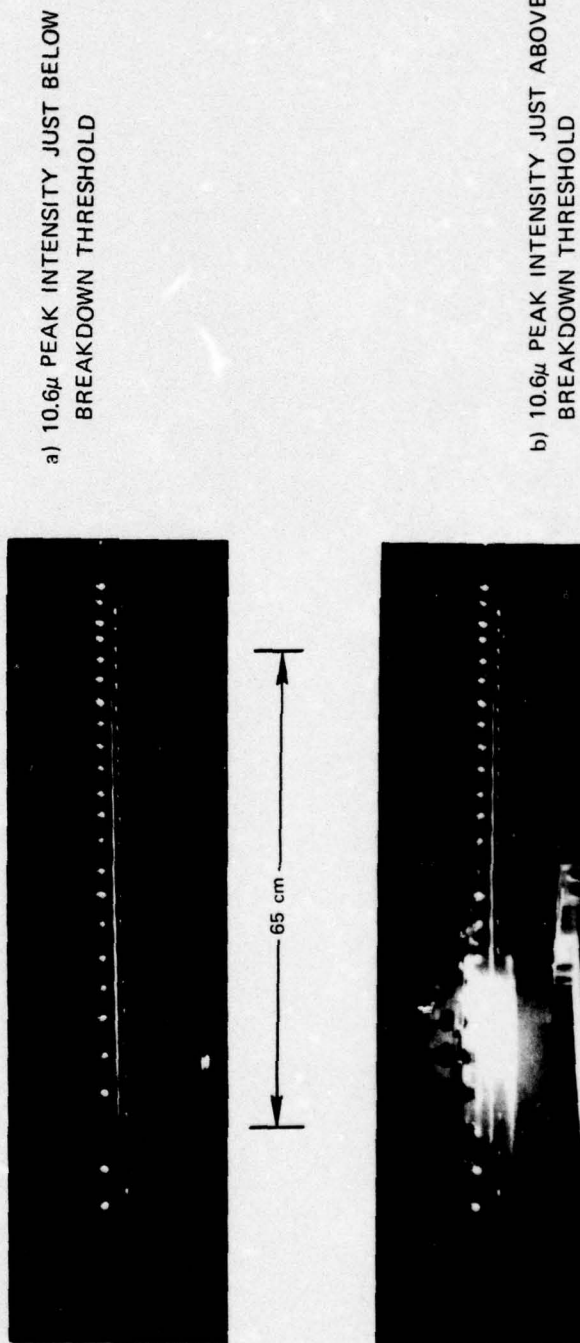
OPTICALLY–PUMPED uv LASER SIGNALS

(AMPLIFIED SPONTANEOUS EMISSION MODE)

a) LASER SPOT ON FLUORESCENT SCREEN
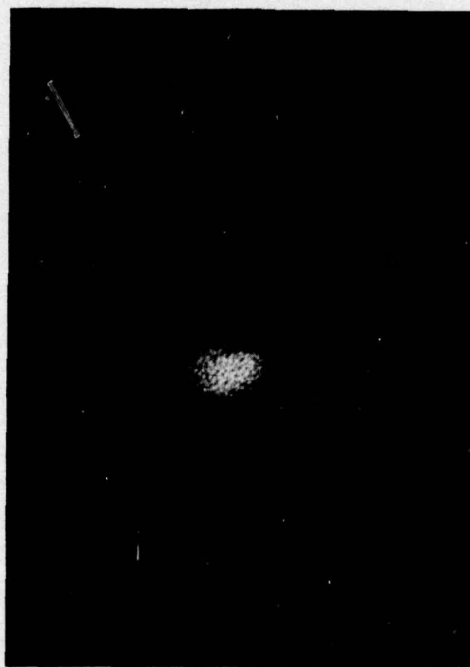
b) 3371Å LASER PULSE

c) 10.6μ PUMPING PULSE

2.5x10 UNITS/DIV

FIG. 4.5

uv LASER SIGNAL IN He/N$_2$

p = 1.5 atm

SECTION 5

CHARGE TRANSFER SYSTEM

5.1 Introduction

In Section 4, it was pointed out that the second positive system in nitrogen has limited efficiency due to the large number o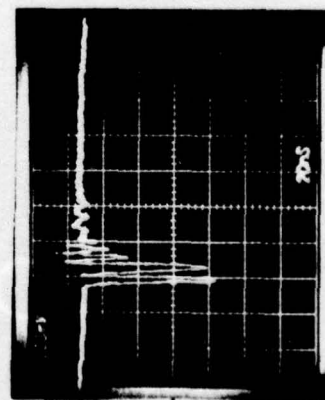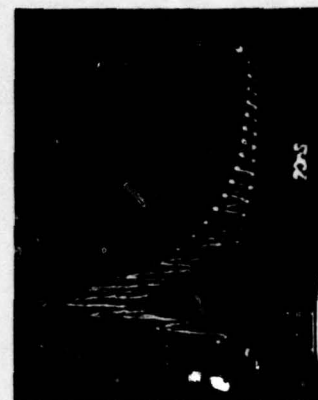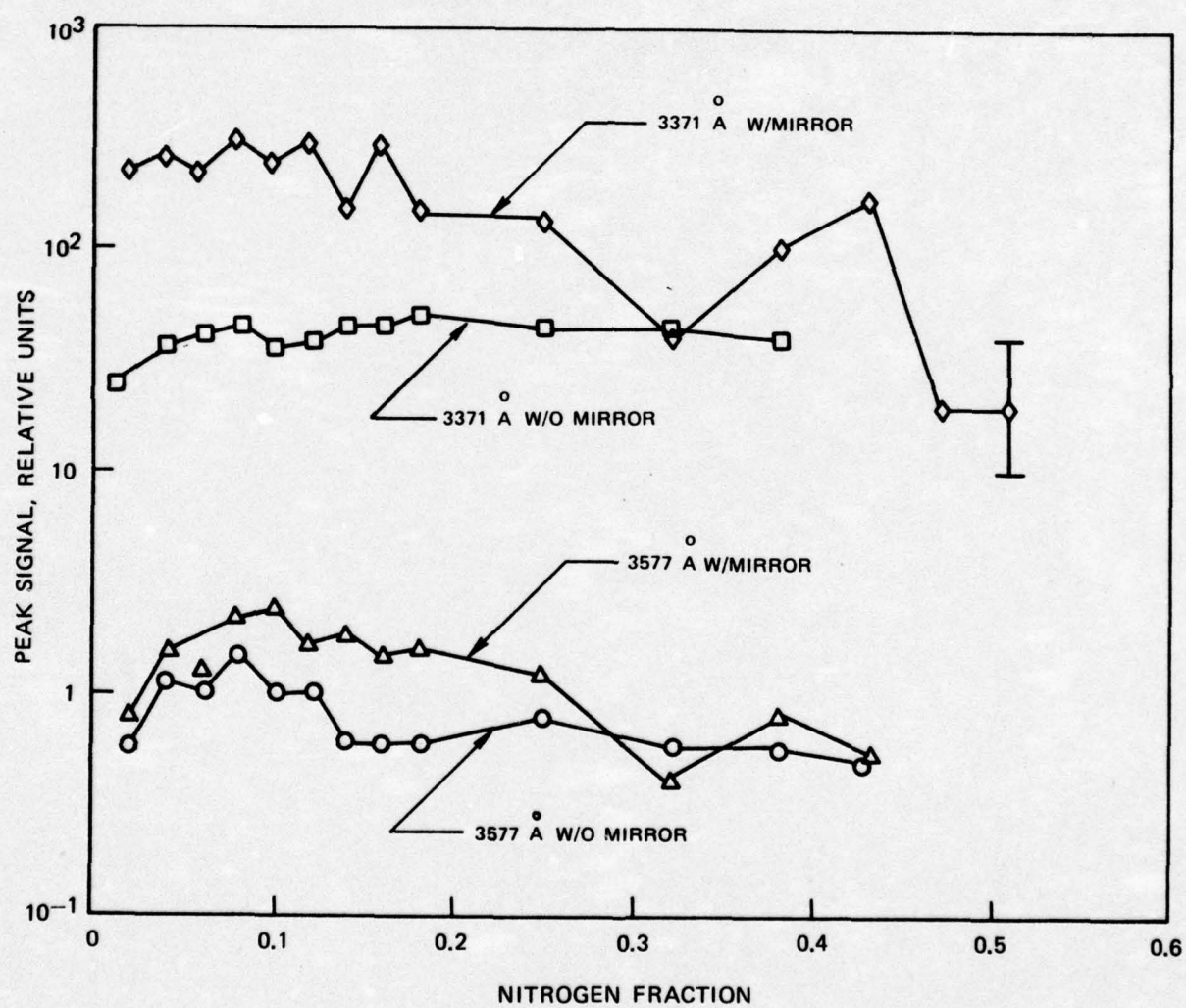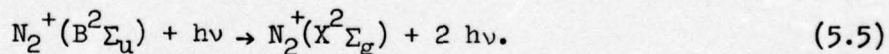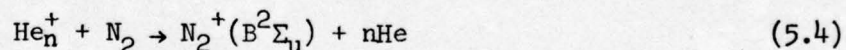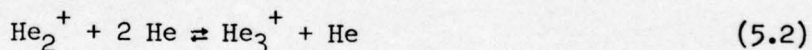f electron energy loss processes in the vicinity of the upper laser level. One way of overcoming this problem would be to operate in a system where a large fraction of the electron energy preferentially channels into the upper level, or channels into a state which can transfer energy to the upper level. One such system is the charge transfer system, which has been investigated with e-beam excitation by Collins, et. al. (CCLC, WCC, CC). The relevant energy levels for the He-N_2 system are shown in Fig. 4.1.

At high helium pressures (e.g., > 10 atm), low N_2 pressures (e.g., 10-50 torr) and high electron energies, the primary electron energy loss is to He ionization. The pumping reaction sequence is then

$$He^+ + 2\,He \rightarrow He_2^+ + He \tag{5.1}$$

$$He_2^+ + 2\,He \rightleftharpoons He_3^+ + He \tag{5.2}$$

$$He_3^+ + 2\,He \rightleftharpoons He_4^+ + He \tag{5.3}$$

$$He_n^+ + N_2 \rightarrow N_2^+(B^2\Sigma_u) + nHe \tag{5.4}$$

$$N_2^+(B^2\Sigma_u) + h\nu \rightarrow N_2^+(X^2\Sigma_g) + 2\,h\nu. \tag{5.5}$$

Collins demonstrated lasing on several vibrational components of this transition, with the strongest lasing occurring on the (0,1) component at 427.8 nm.

While it is well known that high energy electron beams deposit a large fraction of their energy in the form of ionization (WCC), it is also reasonable to expect that for the gas mixture and pressure mentioned above, the same effect would occur in a discharge, provided the electron temperature can be driven to a high enough value. This effect has been verified experimentally in a blumlein discharge operating at total pressures of 2 to 5 atmospheres and nitrogen concentrations of 0.1 percent to 0.2 percent, in which superradiant stimulated emission was obtained from molecular-nitrogen ions at 391.4 and 427.8 nm (LF75).

5.2 Studies at 427.8 nm in He/N_2 Mixtures

A number of experiments were carried out to look at this same process in the optically-pumped discharge. Since it was desired to study the kinetics in a

configuration which allowed efficient coupling from the 10.6 μ field to the discharge, and since it was desirable to be able to use an optical cavity, the studies were carried out using the configuration in Fig. 3.4.

Typical results are shown in Fig. 5.1. The discharge was very uniform and diffuse, and could be operated at N_2 pressures in the 10 torr - 100 torr range, corresponding to the optimum conditions under e-beam excitation. The fluorescence was viewed end-on through a quartz window, with a narrow band (9 nm hw) filter over the detector. The fluorescence was quite intense, and showed a fast risetime, indicating that the transfer sequence (5.1 - 5.4) occurred on a time scale short compared to the pumping pulse. However, using a stable cavity at 427.8 nm, with a 4 meter radius 99.5 percent reflecting mirror, and a 95 percent reflecting flat output mirror, no lasing was observed. A parametric study indicated that the maximum fluorescence occured at a nitrogen pressure of 10 torr, however lasing could not be observed for N_2 pressures from 5 torr to 80 torr.

In order to gain more insight into the kinetics of the discharge and to investigate the lack of lasing, fluorescence spectra were taken, and typical results are shown in Fig. 5.2. This figure shows that the (0,1)-427.8 nm and (0,0)-391.4 nm transitions are very strong, but that a large number of electronic levels of the nitrogen molecule, in particular the second positive system, were also excited. This indicates that the electron temperature was too low, and that a large fraction of the electron energy was going into electronic excitation of the nitrogen, rather than into ionization of the helium. This effect is shown in Fig. 5.3 in which the fluorescence signals are plotted for various N_2 fractions, and, as expected, increasing the nitrogen fraction increased the fraction of electron energy going into electronic excitation. The lack of lasing at the low N_2 concentration was evidently due to too small a concentration of molecules in the $B^2\Sigma_u^+(0)$ state, and was also due to the rather short effective gain length associated with the plasma-sweeping effect discussed in Section 3.4.

In order to investigate these effects further, experiments were carried out in a blumlein discharge channel, which was based on the design of von Bergmann (VHP75). Because of structural limitations, high pressures, such as those used in Ref. (LF75), could not be used. However, measurements were made at pressures up to 1 atm, and provided additional insight into the charge transfer kinetics. A diagram of the discharge channel is shown in Fig. 5.4, and typical spectra for the He/N_2 mixtures are shown in Fig. 5.5-a. It can be seen that fewer electronic levels were excited in the blumlein discharge than in the optically-pumped discharge, but that there was still considerable excitation of the $C^3\pi$ level. It is possible that some of this fluorescence was produced by cascade processes following recombination of the nitrogen ions, however, time resolved measurements at 337.1 nm suggested that it was due to direct electron collisional excitation. The conclusion to be drawn from Fig. 5.5 is that the effective E/n in the blumlein discharge is very high, so that production of He+ and subsequent charge transfer are favored, even though the total pressure is much lower than in the optically-pumped discharge studies.

5.3 Studies at 421.0 nm in He/CO Mixtures

As seen from Fig. 5.1, the decay time of the 427.8 nm fluorescence was $\sim$ 40 nsec. With an optical cavity length of 1.5 m, this allowed only $\sim$ 4 round trips for 427.8 nm flux building up in the cavity, and even fewer round trips during the period of maximum upper state population. Thus, it was desirable to look at systems which had a longer decay time, such as the He/CO charge transfer system (WCC75).

This system was investigated both in the optically pumped discharge and in the blumlein discharge. Figure 5.6 shows that the fluorescence decay time at 421.0 nm was in fact quite long, but that the bulk of the electron energy went into CO electronic levels directly, rather than into CO^+, via charge transfer. The same result was observed in the blumlein discharge. Attempts to obtain lasing in the optically pumped discharge, with a cavity optimized at 421.0 nm, were not successful.

FIG. 5.1

DISCHARGE FLUORESCENCE AT 4278Å

$p = 16.7$ atm, $p_{N_2} = 30$ torr
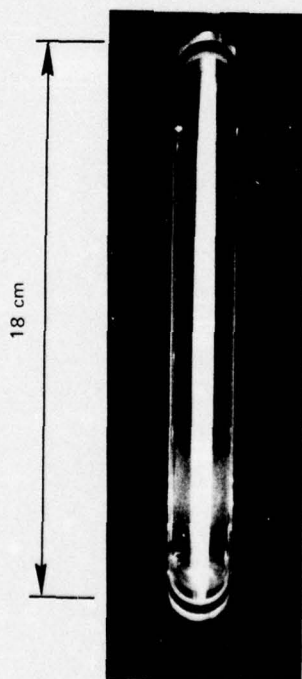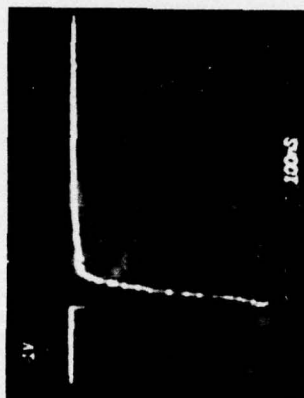
(b) FLUORESCENCE AT 4278Å

18 cm

(a) DISCHARGE

FIG. 5.2

FLUORESCENCE SPECTRA FROM OPED IN He/N$_2$

p_{N_2} = 40 torr, p_{He} = 17 atm, NO TAIL ON TEA PUMPING PULSE
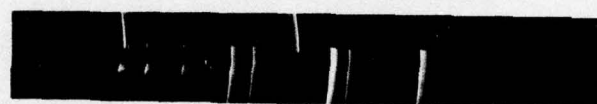
Hg CALIBRATION
OPED FLUORESCENCE

357.7 nm   337.1 nm
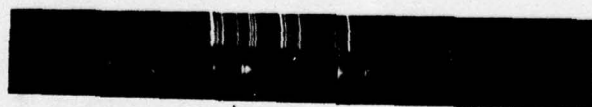
$C^3\Pi_u(0) - B^3\Pi_g(1)$ $C^3\Pi_u(0) - B^3\Pi_g(0)$

Hg CALIBRATION
OPED FLUORESCENCE

427.8 nm   391.4 nm

$B^2\Sigma_u^+(0) - X^2\Sigma_g^+(1)$ $B^2\Sigma_u^+(0) - X^2\Sigma_g^+(0)$

FIG. 5.3

FLUORESCENCE SIGNALS

(He/N$_2$ AT 17.0 atm)

FIG. 5.4
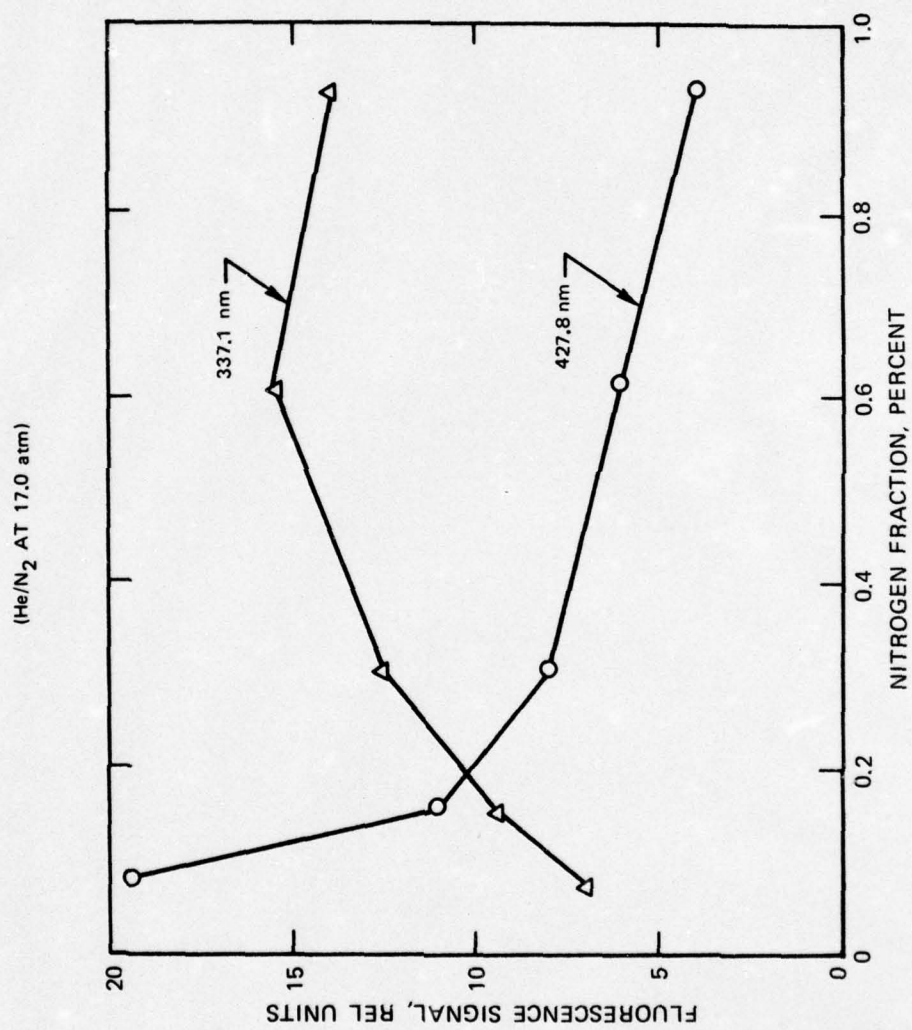
SCHEMATIC DIAGRAM OF BLUMLEIN DISCHARGE

FIG. 5.5
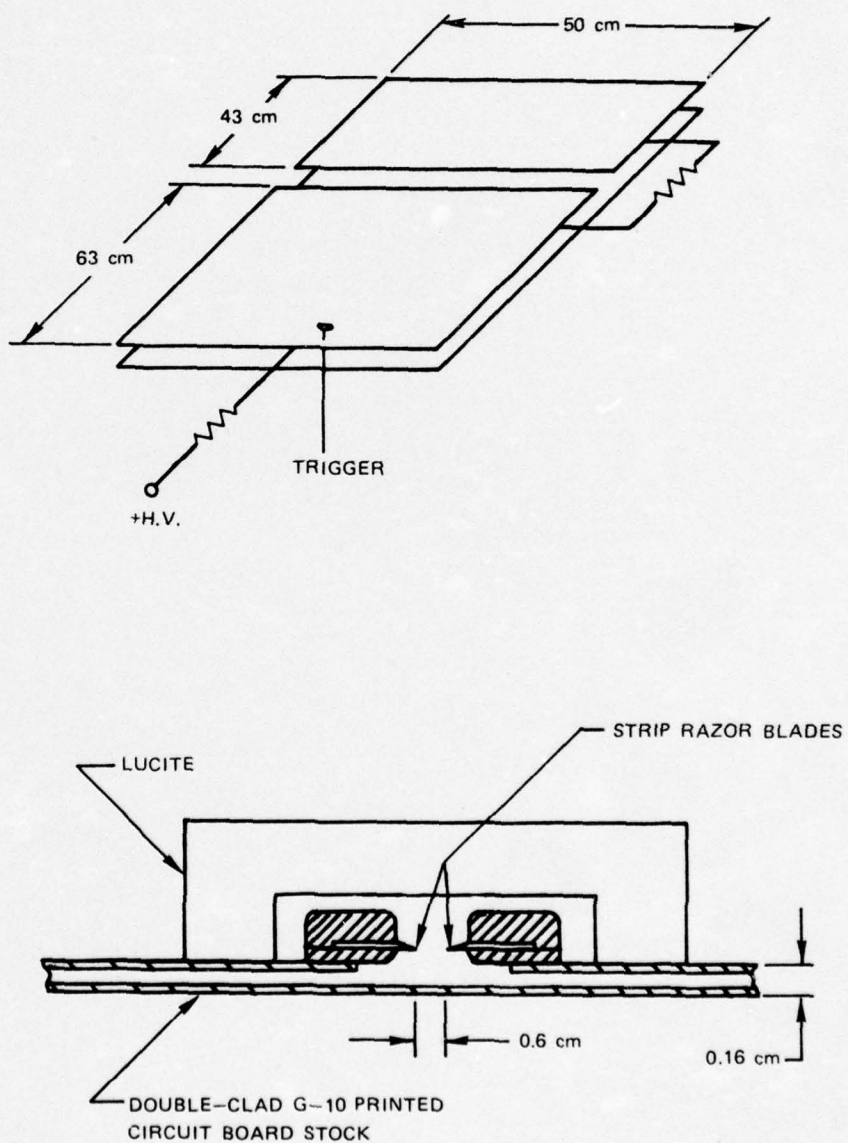
FLUORESCENCE SPECTRA FROM BLUMLEIN DISCHARGE

(a)

He/N_2 MIXTURE
p_{N_2} = 1.5 torr
p_{He} = 1.0 atm

427.8 nm
$B^2\Sigma_u^+$ (0)–$X^2\Sigma_g^+$ (1)

391.4 nm
$\beta^2\Sigma_u^+$ (0) – $X^2\Sigma_g^+$ (0)

337.1 nm
$C^3\Pi_u$ (0) – $B^3\Pi_g$(0)
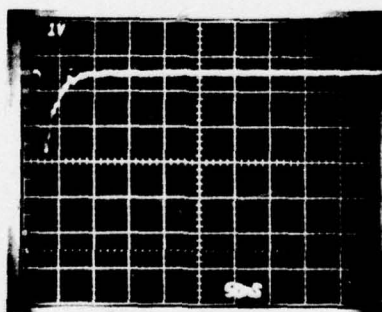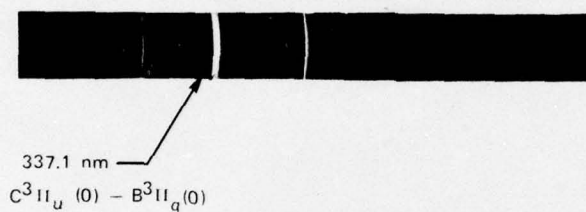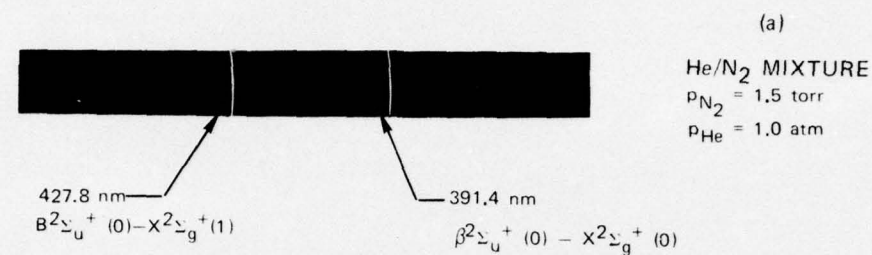
FLUORESCENCE PULSE,
WITH NARROW–BAND
FILTER AT 427.8 nm
(9.0 nm HALFWIDTH)

(b)

He/CO MIXTURE
p_{CO} = 1.5 torr,
p_{He} = 1.0 atm

389.3
HERTZBERG (0–1) BAND

FIG. 5.6
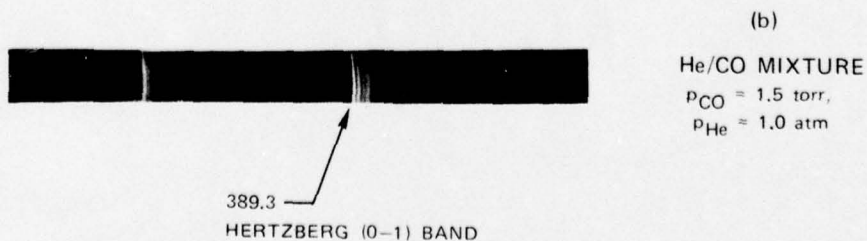
FLUORESCENCE SPECTRA FROM OPED IN He/CO

$p_{CO} = 10$ torr, $p_{He} = 17$ atm, NO TAIL ON TEA PUMPING PULSE

Hg CALIBRATION

OPED FLUORESCENCE

421.0 nm

389.3 nm

B → A (0,1) BALDET −
JOHNSON CO$^+$

HERTZBERG (0−1) BAND
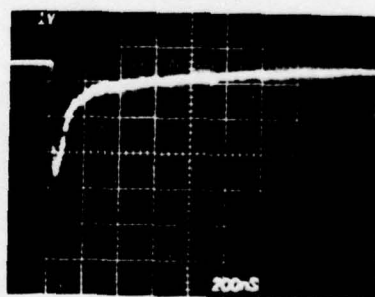
FLUORESCENCE PULSE,
WITH NARROW−BAND
FILTER AT 421.0 nm
(8.0 nm HALFWIDTH)

SECTION 6

RARE GAS HALIDE SYSTEMS

6.1 Introduction

The rare gas halide systems have shown the potential for high efficiency under proper electrical excitation, and have been operated in the pure discharge-pumped mode. Therefore these systems are attractive candidates for the optically pumped discharge approach. It has recently been shown (LHHMN76) that it may be desirable to operate rare-gas-halide systems at high pressure (> 20 atm) in order to shift the lasing transition into the visible range (410 nm vs 248 nm). Since the optically pumped discharge is one of the few discharge techniques capable of operating at very high pressures, this approach might prove useful as an excitation method in rare-gas-halide systems.*

6.2 Optically-Pumped Discharges in the Presence
of an Electronegative Gas

As discussed previously, an inherent part of the present experimental approach was the use of photo-preionization. Given the large cross section for electron attachment, typical of halogenated molecules (Ch71), it was not clear that the uv preionization would be effective in the presence of F_2. In order to investigate this problem, conditions similar to those in Fig. 5.1 were run, but with a small fraction of F_2 added. The results are shown in Fig. 6.1, which shows a photograph of the discharge and a detector trace showing the relative delay between the pre-ionization and the TEA pumping pulse. This photograph and others, to be described below, show that the uv preionization is indeed very effective, even in the presence of a strong electron attacher. For the optically pumped discharge to form, it is necessary to have free electrons to participate in the inverse bremsstrahlung process; and the photograph shows that even after ~ 2 μsec, there was a substantial level of electron density, uniformly distributed over the focal volume.

6.3 Studies in F_2/Xe/He Mixtures

A large number of tests were carried out to examine the potential for operating the OPEDL on the 354 nm transition in XeF. A photograph of a typical discharge is

---

*At the time that the present experiments were carried out, the results regarding the 410 nm band were not published, and conditions appropriate to optimizing this wavelength region were not investigated in the present study.

shown in Fig. 6.2. The discharges obtained with these gas mixtures were very uniform and very repeatable. For these tests, the delay between the preionization and the pumping pulse was reduced to ~ 0.5 µsec, the xenon pressure was chosen comparable to that used in discharge excited XeF lasers (BPD76), and the F_2 pressure was varied as a parameter.

The cell and gas handling system used in these experiments were made of stainless steel and were sealed with viton O-rings. The 10.6 µ input window was AR-coated germanium, and the visible windows were quartz. The cell was passivated by filling it with a mixture of 10 percent F_2, 90 percent He at 1 atm and allowing the system to stand for several hours. The cell was operated for many hours with various pressures of F_2, and none of the components showed any degradation due to F_2. In the uv cavity experiments, to be described later, it was found that the max-R uv mirror (dielectric coating on a fused silica substrate) showed no signs of attack by F_2, but that the partially transmitting uv mirror showed a slight fogging, and had to be replaced by a mirror external to the cell, as shown in Fig. 3.9.

In running the experiments, the cell was purged with dry nitrogen after each shot in order to remove any aerosols produced by the preionization spark or by the 10.6 µ radiation striking the inside of the cell. The cell was then pumped out to ~ 10^{-4} torr and refilled with the appropriate gas mixture. After various shots, samples of the gas were analyzed, using a wet chemistry technique, to check the F_2 concentration against that determined from the pressure gauges used in filling the cell. The values agreed to within 50 percent indicating a minimal loss of F_2 due to chemical reactions.

As discussed in Section 3, the coupling efficiency into the discharge increases with increasing total pressure, and the helium pressure was therefore set at the highest value allowed by the structural strength of the cell. The helium did not appear to quench the XeF* level, even up to pressures of 20 atm, as shown in Fig. 6.3

A typical spectrum of the XeF* discharge is shown in Fig. 6.4, and is compared with that obtained with e-beam pumping. The band structure is very similar to that obtained with e-beam pumping, and the 354 nm band is only slightly broader with the optically pumped discharge. Considering the much higher pressure in Fig. 6.4-a, this indicates that the spectral bandwidth is determined by spin-orbit splitting, as discussed in Ref. (BE75-2) rather than by collision broadening. The XeF* fluorescence at 350 nm was the only fluorescence from the discharge, with the exception of a very weak band at 420-490 nm.

A quantitative estimate of the [XeF*] density was made using an apertured, calibrated photodetector, and using the spontaneous emission rate for XeF* given in Ref. (BE75-2). The value corresponding to the peak of the fluorescence pulse was [XeF*] ~ 2 x 10^{14} cm^{-3}, and, using the cross section for stimulated emission from

Ref. (BE75-2) of $\sigma_{STE} = 2.6 \times 10^{-16}$ cm^2, the peak gain at 354 nm was estimated to be 0.05 cm^{-1}. (Assuming no population of the lower level.) The fluorescence pulse shape corresponding to Fig. 6.4-a was identical to that shown in Fig. 6.3-c. With this level of gain, over the dimensions indicated by the photo in Fig. 6.2-b, the system should be above the lasing threshold, in the presence of a high Q optical cavity.

The optical cavity arrangement shown in Fig. 3.9 was used with a 99.5 percent reflecting curved reflector and a 95 percent reflecting flat output coupler, but no indication of lasing was obtained. This negative result was probably related to the following effects. (1) The effective gain duration, as seen from Fig. 6.3-c, was ~ 40 nsec, allowing only ~ 4 round trip transits of the uv cavity flux. (2) The effective gain length as discussed in Section 3.4, may have been much shorter than the 30 cm length indicated by Fig. 6.2-b. (3) The high electron densities (~ 3×10^{15} cm^{-3}) encountered in these experiments may have led to the formation of absorbing species, or may have caused filling of the lower laser level via quenching.

Since the traces with the discharge viewed end on effectively gave a time integrated picture of the fluorescence, traces were also taken with the detector viewing the discharge side-on. Figure 6.5-a shows that at a given point along the discharge axis, the duration of the XeF* fluorescence was ~ 20 nsec. A similar time scale is shown in Fig. 6.6-b, in which the transmitted 10.6 μ signal, and the side fluorescence signal at 354 nm have been superimposed on the same trace. For comparison, the incident 10.6 μ pulse shape is shown in Fig. 6.6-a. In this run, the detector viewed the window second from the right, as seen in Fig. 6.2-a. The uv pulse corresponds to the plasma sweeping by the window, and indicates that there was ~ 10 nsec delay between the pumping pulse and the XeF* fluorescence. Using the F_2 quenching rate for XeF* of 8×10^{-10} cm^3/sec, quoted in Ref. (BE75-2), we obtain a decay time of 35 nsec for quenching by F_2. Since the measured decay time was shorter than this, and was shorter than the spontaneous decay time of 50 nsec, quoted in Ref. (BE75-2), it is likely that the decay time seen in Fig. 6.6-b, was due to electron quenching. This conclusion is consistent with the electron quenching rate of 2×10^{-8} cm^3/sec listed in Ref. (BE75-2).

6.4 Studies in F_2/Kr/He Mixtures

A partial energy level diagram for the KrF system is shown in Fig. 6.7, where the potential energy curves for KrF have been taken from Ref. (DH76). Since the lower laser level for the $^2\Sigma_{\frac{1}{2}} \rightarrow ^2\Sigma_{\frac{1}{2}}$ transition at 249 nm is unbound, and since in a mixture of 1 torr F_2, 10 torr Kr, 17 atm He, and $\bar{u}_e \sim 2$ eV, we expect the dominant electron energy loss to be excitation of the ^1P, ^3P krypton manifold, this system is a good candidate for use with the OPEDL approach.

Diffuse discharges were again obtained in mixtures of $F_2/Kr/He$, with the discharge appearing similar to that in Fig. 6.2-b. A typical spectrum is shown in Fig. 6.8, and it can be seen that the fluorescence is again very similar to that obtained with e-beam pumping. For these conditions, emission at 249 nm was the only fluorescence observed with an f3.5 optical train, with a 40 μ entrance slit on the spectrograph, with Polaroid Type 57 film, and with single shot operation. It should be noted that high Kr pressures, at which one would expect to see the Kr_2F^* fluorescence discussed in Ref. (LHHMN76), were not investigated in the present study.

The sequence of photos of the discharges, obtained in making the spectral scan of the $F_2/Kr/He$ mixtures, vividly illustrate the uniformity and repeatability of the discharges under these conditions and are shown in Fig. 6.9.

The effect of F_2 quenching on the fluorescence decay time is shown in Fig. 6.10 and indicates that the F_2 quenching rate for KrF^* is approximately the same as that quoted above for XeF^*.

Since the expected cross section for stimulated emission in KrF is smaller than that for XeF, due to the greater width of the emission band, and since mirrors optimized for 249 nm were not on hand, no attempt was made to obtain lasing at this wavelength.

Using a calibrated detector and an aperture, as for the XeF case, the efficiency of conversion from 10.6 μ energy to fluorescence at 249 nm was measured to be 0.1 percent. This low value (compared to that observed with e-beam pumping) was probably due to electron quenching.

FIG. 6.1

DISCHARGE IN He/N$_2$/F$_2$ MIXTURE

$p_{F_2} = 5$ torr, $p_{N_2} = 20$ torr, $p_{He} = 250$ psia

— TEA PUMPING PULSE

— PREIONIZING PULSE

FIG. 6.2
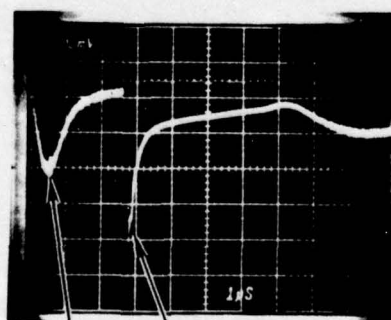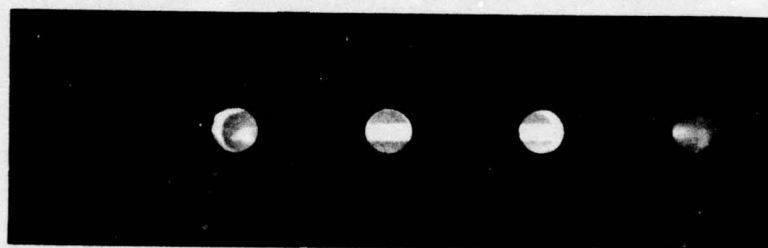
DISCHARGE IN He/F$_2$/Xe MIXTURE

p_{F_2} = 1 torr, p_{Xe} = 10 torr, p_{He} = 20 atm

(a)

PHOTO OF CELL

25 cm

(b)
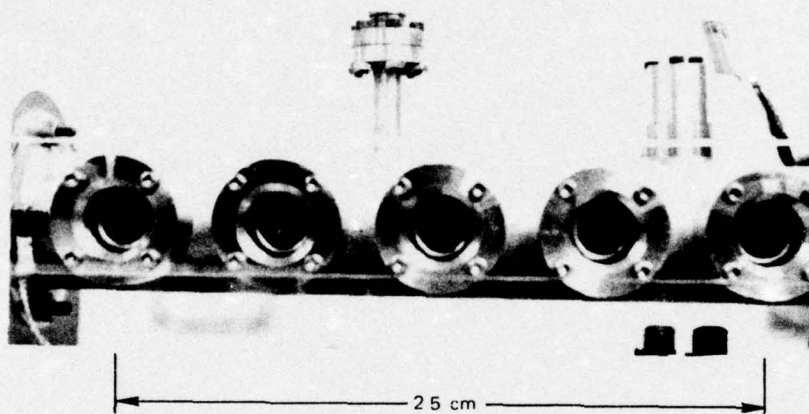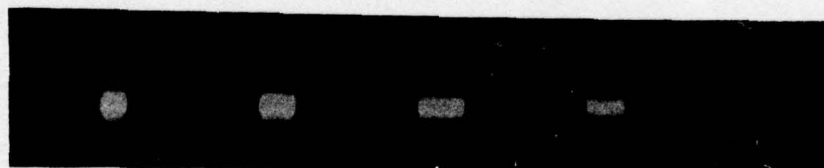
PHOTO OF
DISCHARGE
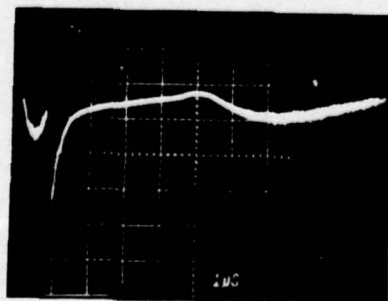
(c)

TIMING SEQUENCE

TEA PUMPING PULSE

PREIONIZING PULSE

76–09–185–1

FIG. 6.3

EFFECT OF He PRESSURE ON KrF* FLUORESCENCE DECAY TIME

$p_{Kr} = 10$ torr, $p_{F_2} = 0.1$ torr

NO TAIL ON TEA PUMPING PULSE
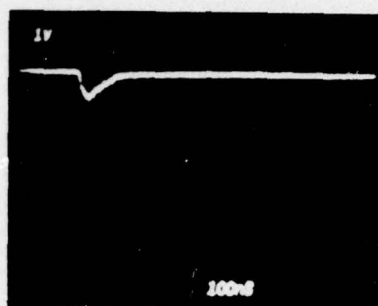
(a) $p_{He} = 4.2$ atm
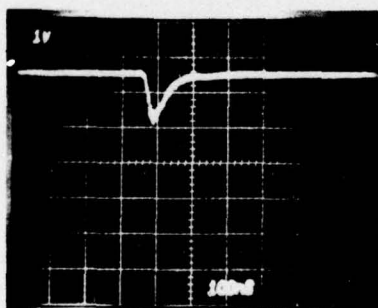
(b) $p_{He} = 8.5$ atm

(c) $p_{He} = 17$ atm

FIG. 6.4
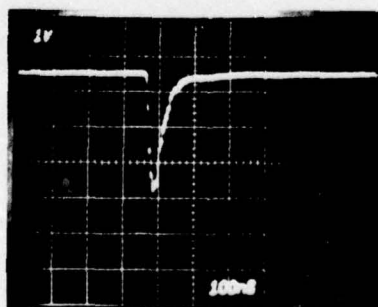
FLUORESCENCE SPECTRUM IN F_2/Xe/He MIXTURE

(a)

SPECTRUM OF XeF^* IN
OPTICALLY—PUMPED DISCHARGE

p_{F_2} = 1 TORR, p_{Xe} ≈ 10 torr, p_{He} ≈ 20 atm

WAVELENGTH, nm

OPED FLUORESCENCE

Hg CALIBRATION

(b)

SPECTRUM OF XeF^* IN
e—BEAM EXCITED MIXTURE
(FROM REF. BE75-1)

(Ar + 10% Xe + 1% F_2, 776 torr)

WAVELENGTH (nm)
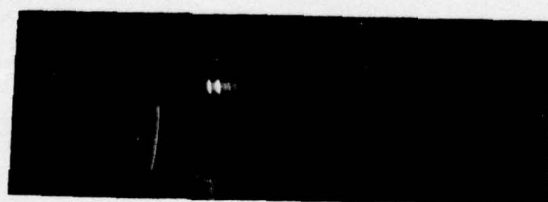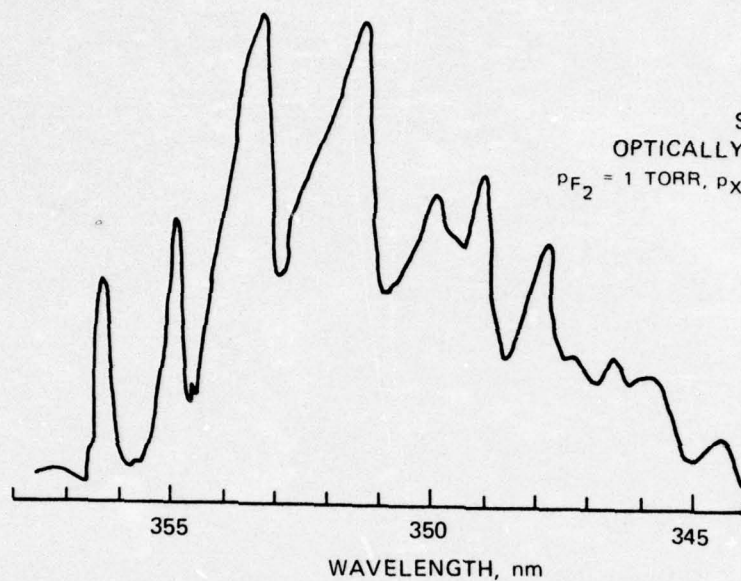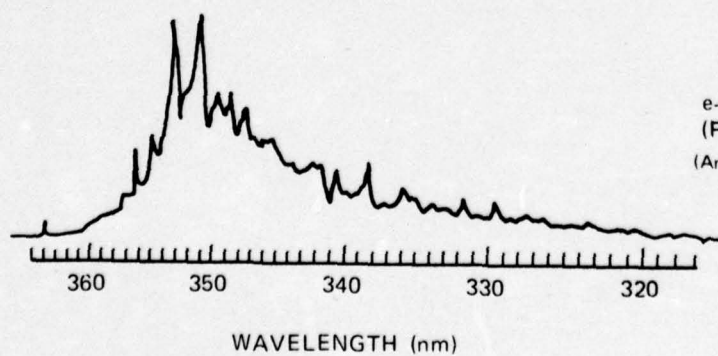
FLUORESCENCE SIGNAL IN F_2/Xe/He

$p_{F_2} = 10$ *torr*, $p_{Xe} = 10$ *torr*, $p_{He} = 17$ *atm*

NO TAIL ON TEA LASER PULSE
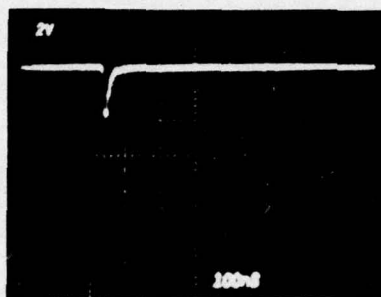
(a)

DETECTOR LOOKING SIDE–ON

(ARBITRARY VERTICAL SCALE)
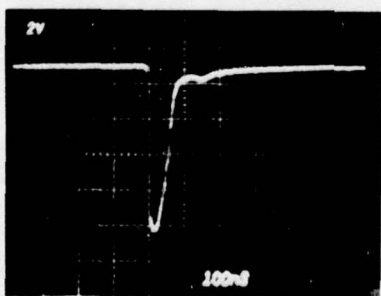
(b)

DETECTOR LOOKING END–ON

(ARBITRARY VERTICAL SCALE)

FIG. 6.6

RELATIVE TIMING BETWEEN PUMPING PULSE AND XeF* FLUORESCENCE PULSE

P_{F_2} = 1 TORR, P_{Xe} = 10 torr, P_{He} = 17 atm
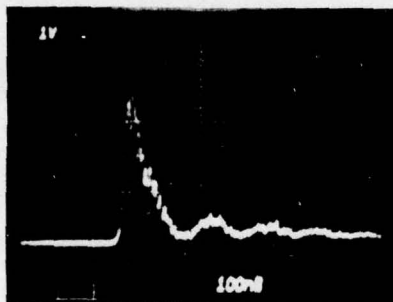
(a) INCIDENT
10.6μ PULSE
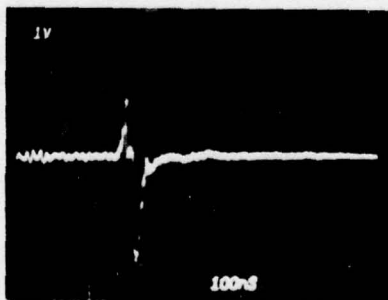
(b) TRANSMITTED
10.6μ PULSE + XeF*
SIDE FLUORESCENCE
PULSE

PARTIAL ENERGY LEVEL DIAGRAM FOR F_2/Kr/He SYSTEM

FIG. 6.8
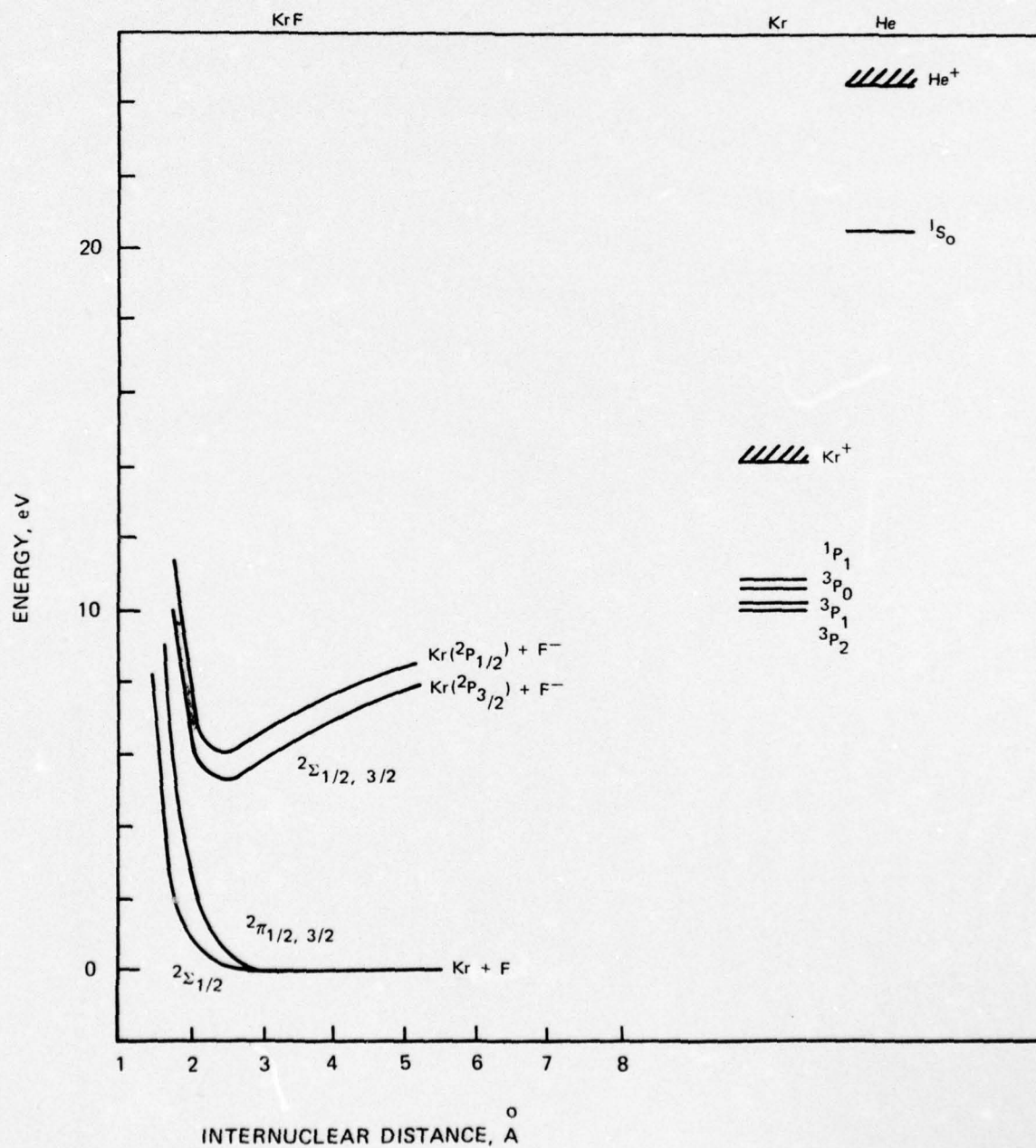
FLUORESCENCE SPECTRUM IN F_2/Kr/He MIXTURE
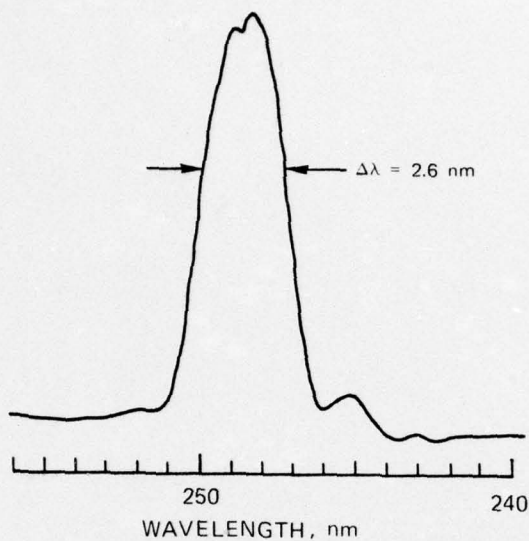
(a)

SPECTRUM OF Kr F* IN
OPTICALLY-PUMPED DISCHARGE

p_{F_2} = 10 torr, p_{Kr} = 10 torr,

p_{He} = 17 atm

$\Delta\lambda$ = 2.6 nm

250   240

WAVELENGTH, nm

OPED FLUORESCENCE

Hg CALIBRATION

KrF$(^2\Sigma_{1/2} - {}^2\Sigma_{1/2})$ EMISSION SPECTRUM

$\Delta\nu$ = 400 cm^{-1}

$\Delta\lambda$ = 2.0 nm
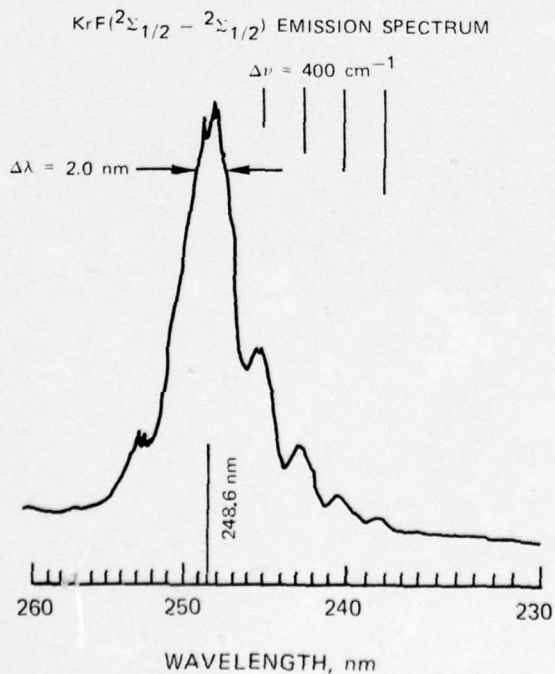
(b)

SPECTRUM OF KrF* IN e–BEAM
EXCITED MIXTURE (FROM REF.
BE75–1)

p_{F_2} = 2 torr, p_{Kr} = 20 torr,

p_A = 2.7 atm

248.6 nm

260   250   240   230

WAVELENGTH, nm

FIG. 6.9

DISCHARGES IN $F_2/Kr/He$

$p_{F_2} = 10$ torr, $p_{Kr} = 10$ torr, $p_{He} = 17$ atm

FIG. 6.10
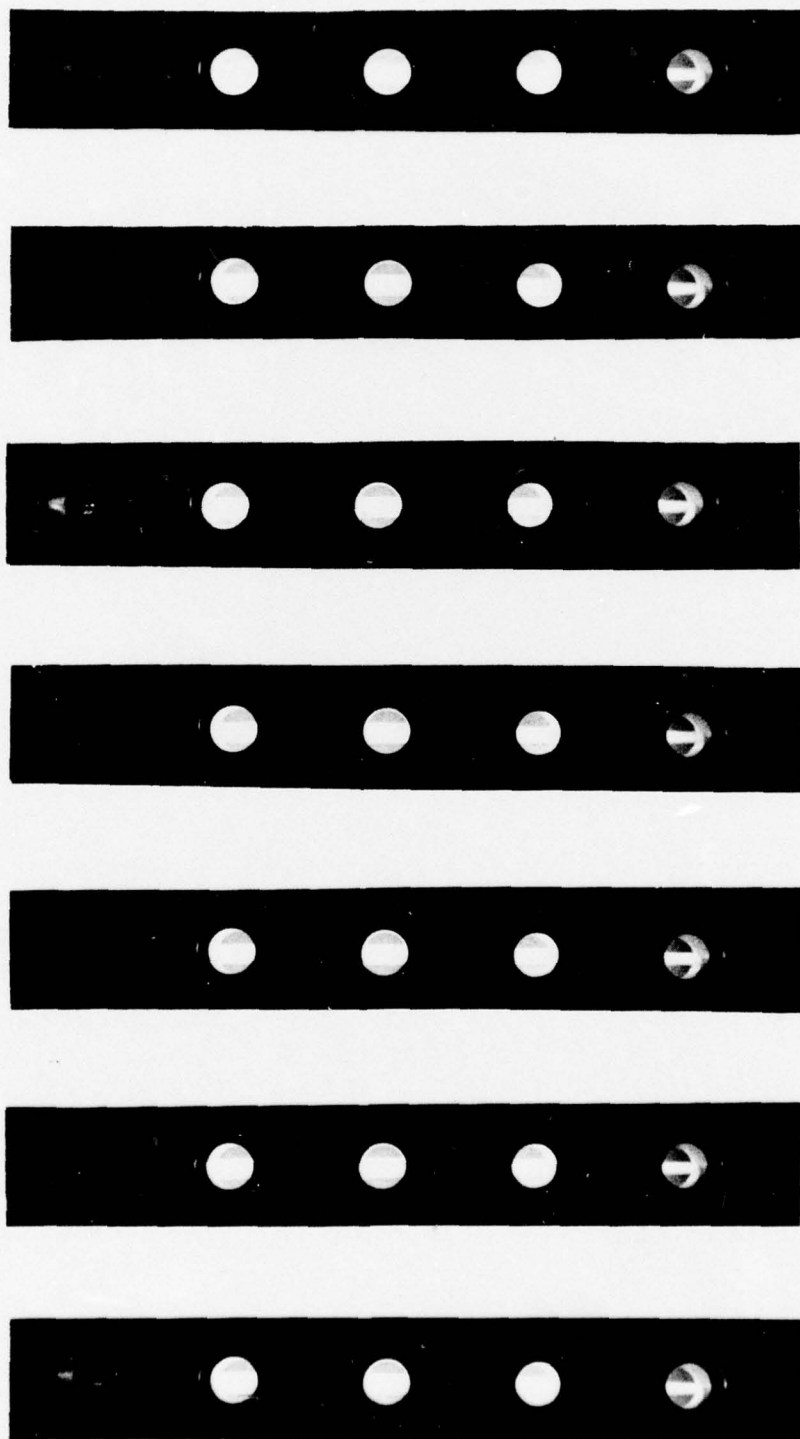
EFFECT OF F$_2$ PRESSURE ON KrF* FLUORESCENCE DECAY TIME

p_{Kr} = 10 torr, p_{He} = 17 atm

NO TAIL ON TEA PUMPING PULSE
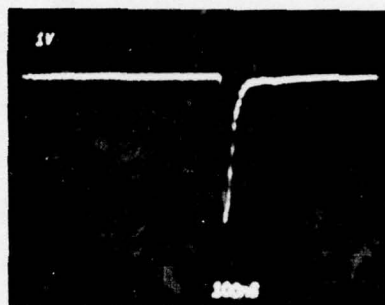
(a) p_{F_2} = 10 torr
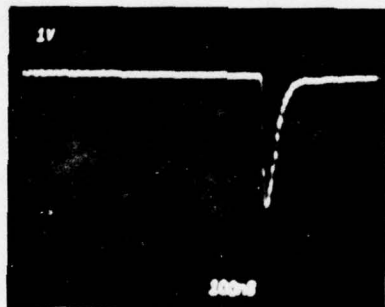
(b) p_{F_2} = 1 torr
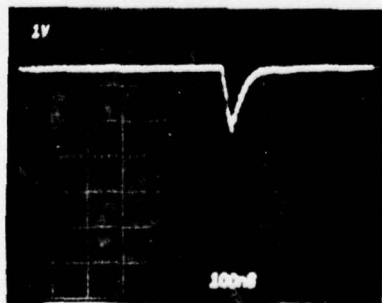
(c) p_{F_2} = 0.1 torr

SECTION 7

CONCLUSIONS AND RECOMMENDATIONS

It has been shown that the optical pumping technique is capable of generating large-volume, high density discharges in a variety of gases, using simple photo-preionization. An optical configuration was developed which allowed the incorporation of a uv optical cavity, and at the same time allowed over 95 percent of the 10.6 μ radiation to be coupled into the discharge. The optimum discharge configuration showed good scalability, showed high-repetition rate capability, and was operated in a variety of gas mixtures, including those containing F_2, at pressures up to 20 atm.

Studies aimed at demonstrating high-efficiency lasing were not successful. Lasing at 337.1 nm was demonstrated, but with very low efficiency. This low efficiency was due to the inherent low efficiency of the N_2 second positive system, and to inefficient optical coupling. Experiments with the He/N_2 charge transfer system indicated that the electron temperature was too low, resulting in the excitation of various electronic levels, rather than the desired formation of helium ions. Studies with XeF and KrF showed that the electron density was quite high and indicated that electron quenching was prohibiting efficient formation of the upper laser level.

Based on the results of this study, the following areas are deserving of further study, in order to more completely evaluate the optically-pumped discharge approach.

1. Further studies with transverse pumping-particularly with large area, uniform, multimode beams, and with gases at very high pressures (20-50 atm).

2. Studies of kinetic systems (e.g., metal vapors) compatible with operation at high electron densities.

3. Operation of the He/N_2 charge transfer system with shorter 10.6 pulses, so that higher electron temperatures can be used.

4. Investigation of the KrF system under conditions where lower electron densities are obtained, and in the presence of a good uv optical cavity.

5. Theoretical studies, accounting for the discharge evolution effects outlined in this report.

REFERENCES

BBA76. Bhaumik, M. L., R. S. Bradford, Jr., and E. R. Ault: High-Efficiency
        KrF Excimer Laser. Appl. Phys. Letters $\underline{28}$, 23 (1976).

BE75-1. Brau, C. A. and J. J. Ewing: Emission Spectra of XeBr, XeCl, XeF, and
        KrF. J. Chem. Phys. $\underline{63}$, 4640 (1975).

BE75-2. Brau, C. A. and J. J. Ewing: Excimer Laser Research. AVCO Semi-Annual
        Tech. Rept. on Contract No. N00014-75-C-0063 (August 1975).

BPD76. Burnham, R., F. X. Powell, and N. Djeu: Efficient Electric Discharge
        Lasers in XeF and KrF. Appl. Phys. Letters $\underline{29}$, 30 (1976).

Br74.   Brown, R. T.: Optically Pumped Laser. UARL Rept. N921853-2, Semi-Annual
        Technical Report on ARPA Contract No. N00014-74-C-0376 (October 1974).

Br75-1. Brown, R. T.: Optically Pumped Laser. UTRC Rept. R76-921853-7, Ann.
        Tech. Rept. on ARPA Contract No. N00014-74-C-0376 (October 1975).

Br75-2. Brown, R. T.: Kinetic Processes in a Laser-Heated Helium-Nitrogen
        Plasma for Use as a uv Laser Medium. J. Appl. Phys. $\underline{46}$, 4767 (1975).

BS74.   Brown, R. T. and D. C. Smith: Optically Pumped Laser. Appl. Phys.
        Letters $\underline{24}$, 236 (1974).

CCLC76. Collins, C. B., J. M. Carroll, F. W. Lee, and A. J. Cunningham: Thermal
        Modification of the Kinetic Sequence Pumping the Helium-Nitrogen Charge-
        Transfer Laser. Appl. Phys. Letters $\underline{28}$, 535 (1976).

CC75.   Collins, C. B. and A. J. Cunningham: Scaling of the Helium-Nitrogen
        Charge Transfer Laser. Appl. Phys. Letters $\underline{27}$, 127 (1975).

Ch71.   Christophorou, L. G: Atomic and Molecular Radiation Physics. Wiley-
        Interscience (1971).

DH76.   Dunning, T. H., Jr. and P. J. Hay: Electronic States of KrF. Appl.
        Phys. Letters $\underline{28}$, 649 (1976).

EB75.   Ewing, J. J. and C. A. Brau: Laser Action on the $^2\Sigma_{\frac{1}{2}}^+ \rightarrow {}^2\Sigma_{\frac{1}{2}}^+$ Bands of
        KrF and XeCl. Appl. Phys. Letters $\underline{27}$, 350 (1975).

LF75.   Laser Focus, p. 10 (December 1975).

REFERENCES (Cont'd)

LHHMN76.   Lorents, D. C., R. M. Hill, D. L. Huestis, M. V. McCusker, and
            H. H. Nakano: Spectroscopy and Kinetics of the 248 and 410 nm Bands
            from Electron Beam Pumped Argon-Krypton-Fluorine Mixtures. Presented
            at the Third Summer Colloquium on Electronic Transition Lasers,
            Snowmass in Aspen, Colorado (September 1976).

VHP75.   von Bergmann, H. M., V. Hasson, and D. Preussler: Pulsed Corona
            Excitation of High-Power uv Nitrogen Lasers at Pressures of 0-3 Bar.
            Appl. Phys. Letters $\underline{27}$, 553 (1975).

WCC75.   Waller, R. A., C. B. Collins, and A. J. Cunningham: Stimulated
            Emission from CO^+ Pumped by Charge Transfer from He^+_2 in the Afterglow
            of an E-Beam Discharge. Appl. Phys. Letters $\underline{27}$, 323 (1975).

APPENDIX

Publication Reprints

During this reporting period, the following technical papers, based on this work were published.

1. R. T. Brown, "Kinetic Processes in a Laser-Heated Helium-Nitrogen Plasma for Use as a uv Laser Medium," J. Appl. Phys. 46, 4767 (1975).

2. R. T. Brown, "Optically Pumped Electric Discharge Laser," Presented at the 9th International Quantum Electronics Conference, Amsterdam the Netherlands (June, 1976).

Optically Pumped Electric Discharge Laser[*]

Robert T. Brown
United Technologies Research Center
East Hartford, Connecticut, USA   06108

ABSTRACT

The radiation from a 75 J CO_2 TEA laser was focused into a pre-ionized high-pressure gas to form an intense, diffuse discharge, which served as the active medium for a uv laser. Measurements of uv laser energy and of discharge properties relevant to operation on various uv/visible transitions were made at pressures up to 20 atm.

Optically Pumped Electric Discharge Laser[1]

Robert T. Brown
United Technologies Research Center
East Hartford, Connecticut, USA 06108

The optically pumped electric discharge laser (OPEDL) approach has the
potential of producing high-energy, high-efficiency laser pulses in the uv
and visible portions of the spectrum[2,3]. With this technique the output laser
pulse from a CO_2 TEA laser is focused into the active uv laser medium, which
has been preionized to some low level of electron density. In the present
studies the preionization was produced via photoionization from small arcs
in the uv laser medium. The 10.6μ optical field then heats the electrons via
inverse bremsstrahlung, and the electron density grows in a cascade process.
By properly adjusting the peak intensity of the 10.6μ pumping pulse, the peak
electron density can be held to any desired value short of the gas breakdown
value (the condition in which the 10.6μ absorption length becomes short
compared to the 10.6μ focal volume length). The size of the discharge produced
is determined by the size of the 10.6μ laser focal volume and by the size of
the region illuminated by the preionizing radiation. Since this discharge
can have a very fast risetime and can reach very high electron densities,
the discharge is well suited for pumping various uv and visible laser transitions.

Because of the absence of electrodes, and because of the volumetric
nature of the inverse bremsstrahlung heating process, the optically pumped
discharge is capable of operating at high pressures and is scalable to large
discharge volumes and high repetition rates. This paper will describe ex-

R. T. Brown
Optically Pumped Electric Discharge Laser

periments to study the applicability of this approach to recently developed
laser systems such as the charge transfer laser[4,5] and the rare gas-halide
lasers.[6]

In order to gain better insight into the kinetics of the optically
pumped discharge, and to compare the pumping to that in a conventional dis-
charge and in an electron-beam driven discharge, preliminary experiments were
carried out in high-pressure helium-nitrogen mixtures.[3] These experiments
have recently been extended to much larger focal volumes using a large CO_2
TEA laser and have provided a clear demonstration of lasing on the 337.1-nm
second positive transition in molecular nitrogen. The TEA laser was operated
as an unstable resonator and the beam was focused into the cell with a 2.7 m
focal length mirror. With a mixture of 5% N_2 and 95% He at a pressure of
1.0 atm, the discharge was 0.5 cm in diameter by 42 cm long and produced laser
radiation at 337.1-nm via amplified spontaneous emission. The uv laser pulse
consisted of a series of 4 nsec spikes corresponding to the shape of the self-
modelocked pumping pulse. When a small aluminized mirror was mounted on a
thin strut at one end of the cell, the peak uv laser intensity increased by
a factor of 7, indicating that the amplified spontaneous emission field was
not saturating the transition. Experiments with a longer discharge path
length are presently under way and will be described.

A second series of experiments have recently been carried out using a
multimode beam from the TEA laser, and a 1.5 m focal length focusing mirror,

R. T. Brown
Optically Pumped Electric Discharge Laser

along with a cell configuration allowing the incorporation of a uv optical cavity which is coaxial with the 10.6μ focal volume. Diffuse, high-electron density discharges were obtained in helium, with small fractions of N_2 or CO, at total pressures up to 20 atm. The discharge was cylindrical in shape with a diameter of 1 cm and a length of 22 cm. Measurements of the properties of these discharges in various gas mixtures will be discussed.

Footnotes

[1] Work supported in part by ARPA and monitored by the Office of Naval Research.

[2] R. T. Brown and D. C. Smith, Appl. Phys. Lett. 24, 236 (1974).

[3] R. T. Brown, J. Appl. Phys. 46, 4767 (1975).

[4] C. B. Collins, A. J. Cunningham, S. M. Curry, B. W. Johnson, and M. Stockton, Appl. Phys. Lett. 24, 477 (1974).

[5] R. A. Waller, C. B. Collins, and A. J. Cunningham, Appl. Phys. Lett. 27, 323 (1975).

[6] C. A. Brau and J. J. Ewing, Appl. Phys. Lett. 27, 435 (1975).

Kinetic processes in a laser-heated helium-nitrogen plasma for use as a uv laser medium

Robert T. Brown

United Technologies Research Center, East Hartford, Connecticut 06108
(Received 9 June 1975)

Experimental and theoretical studies of an optically pumped electric discharge laser in helium-nitrogen mixtures are described. While the inherent efficiency of this system is rather low, these studies illustrate the basic parameters controlling the dynamics and efficiency of such a laser. In the experiments, intense diffuse discharges were obtained at pressures up to 12 atm and amplified spontaneous emission along the axis of the discharge was observed. The numerical modeling studies showed qualitative agreement with the experimental data and gave an optimized value of the kinetic coupling efficiency (absorbed 10.6-μ power to uv laser power) of 1.6% and of the total efficiency (energy stored in the TEA laser supply to uv output energy) of 0.1–0.2%.

PACS numbers: 42.60.C, 52.50.J, 52.80.P

I. INTRODUCTION

There is a continuing interest in generating high-energy laser pulses in the uv and visible portions of the spectrum. Previous studies in this area have centered around two techniques for generating such pulses. Low-inductance circuits have been used to produce fast-rising high-current discharges at moderate pressures in order to pump transitions such as the 3371-Å laser transition in molecular nitrogen.[1] More recently, high-energy short-pulse electron beams have been used to produce high-pressure lasers in xenon at 1730 Å,[2] argon/nitrogen at 3577 Å,[3] and helium/nitrogen at 4278 Å.[4] This paper describes experimental and theoretical results of studies using a high-energy 10.6-μ pulse from a TEA CO_2 laser to drive a diffuse discharge in a high-pressure gas. The properties of this discharge are such that it can be used as the active medium for a uv or visible laser and can be used with any of the transitions mentioned above.

The basic concept was described in Ref. 5 along with preliminary experimental results. The present study is an extension of this work to include more detailed measurements of the optically pumped He/N_2 discharge under various conditions, and includes results obtained with a computer model of the kinetic processes in the laser-heated discharge. A comparison between the theoretical and experimental results shows good agreement and leads to considerable insight into the processes controlling the efficiency and scalability of an optically pumped electric discharge laser.

II. EXPERIMENTAL STUDIES

The basic elements of this concept can be explained in terms of the arrangement used in the present experiments, as shown in Fig. 1. The output pulse from the TEA laser was focused into the active uv laser medium which had been preionized to some low level of electron density (in the present study the preionization was produced via photoionization from two rows of small arcs in the uv laser medium). The 10.6-μ optical field then heated the electrons via inverse bremsstrahlung, and the electron density grew in a cascade process.[6] The size of the discharge produced was determined by the size of the volume irradiated by the preionization

arcs and by the 10.6-μ focal volume. Since such a discharge can have a very fast rise time (~10 nsec) and can reach very high electron densities (full ionization, i.e., gas breakdown, for sufficiently high 10.6-μ laser fluxes), this discharge is well suited to pumping various uv laser transitions.

The experimental arrangement used in the present study was similar to that described in Ref. 5, with the exception that the test cell was redesigned to operate at pressures up to 20 atm. The TEA laser was operated in an oscillator/amplifier configuration and produced pulses with 50 MW peak power, 0.5-mrad divergence, and a pulse shape having a 100-nsec-wide leading spike followed by a 1.5-μsec tail. The laser tended to be self-mode-locked, i.e., the pulse consisted of a series of short spikes within the gain-switched pulse envelope.

One of the objectives of these experiments was to study the ionization kinetics over a range of pressures and to determine whether diffuse discharges could be obtained at high pressures. Photographs of typical discharges are shown in Fig. 2. Figures 2(a) and 2(b) were obtained at a pressure p of 7.1 atm and correspond to nitrogen fractions X_{N_2} just below and just above the breakdown threshold (the condition in which the 10.6-μ absorption length becomes short compared to the length of the laser focal volume). A similar effect is seen in Figs. 2(c) and 2(d), obtained at 12.0 atm. In Fig. 2(d), the nitrogen fraction was held constant and the peak 10.6-μ intensity I_0 was increased slightly.[7] The focal
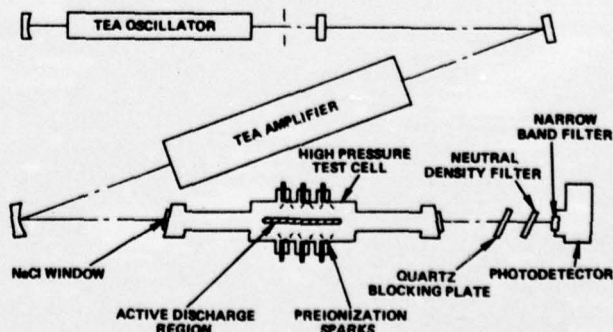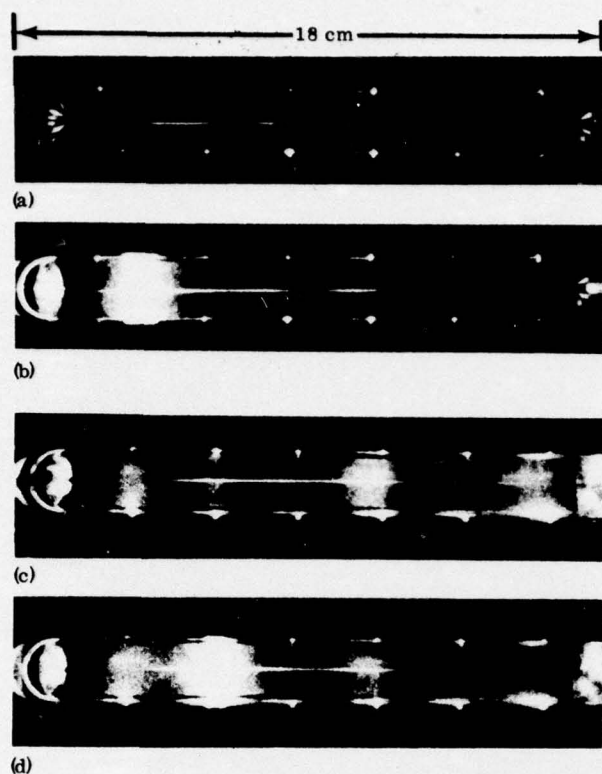

FIG. 1. Diagram of experimental arrangement.

FIG. 2. Photographs of optically pumped discharges in helium-nitrogen mixtures. (a) $p = 7.1$ atm, $X_{N_2} = 0.14$, $I_0 = 1.6 \times 10^9$ W/cm^2. (b) $p = 7.1$ atm, $X_{N_2} = 0.12$, $I_0 = 1.6 \times 10^9$ W/cm^2. (c) $p = 12.0$ atm, $X_{N_2} = 0.13$, $I_0 = 1.2 \times 10^9$ W/cm^2. (d) $p = 12.0$ atm, $X_{N_2} = 0.13$, $I_0 = 1.4 \times 10^9$ W/cm^2.

volume in these experiments had a measured half-power diameter of 1.1 mm and a length of approximately 10 cm. The bright spots in Figs. 2(b) and 2(d) were the result of the diffuse discharge being overdriven, rather than the result of aerosol-induced breakdown, as occurs in laboratory air.[8] Comparison of the properties in Figs. 2(a)—2(d), along with the 10.6-μ absorption measurements in Ref. 6, indicated that the electron

densities in Figs. 2(a) and 2(c) were in the 10^{15}—10^{17}-cm^{-3} range. It can thus be seen that the optically pumped discharge technique is capable of driving high-density diffuse discharges at pressure up to 12.0 atm. It should be noted that this is the only technique, other than the high-energy electron beam, which is capable of generating such discharges. The variation of the electron density with I_0 will be discussed in Sec. III.

A second objective of the experiments was to obtain quantitative data demonstrating laser action on the $C(^3\pi_u)_{v'=0} \rightarrow B(^3\pi_g)_{v=0}$ transition (3371 Å) in an optically pumped He/N$_2$ discharge. In this series of experiments, attempts to incorporate a uv optical cavity into the pumping arrangement were not successful because of the need to isolate the 10.6-μ radiation from the uv radiation and the need to keep these isolating elements well away from the 10.6-μ focus. However, a large number of data were obtained which showed lasing via amplified spontaneous emission.[9]

As shown in Fig. 1, a photodetector with a narrow-band filter at 3371 Å was used to monitor the radiation emitted along the axis of the discharge. Typical traces are shown in Fig. 3. Figure 3(a) was taken with a very low nitrogen fraction and represents the spontaneous emission from the diffuse discharge. The spontaneous emission pulse had approximately the same shape as the TEA laser pumping pulse. Figures 3(b)—3(d) represent increasing values of X_{N_2} (with correspondingly increased values of I_0) and show the development of an amplified-spontaneous-emission spike (note scale changes) with increased nitrogen inversion densities. In Fig. 4, the experimental points were obtained at a fixed pressure and nitrogen fraction, but with increasing values of I_0 and show an exponential increase with
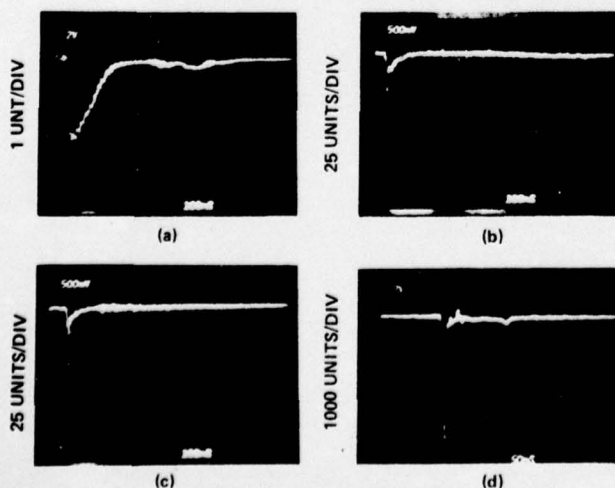

FIG. 3. 3371-Å pulse shortening in He/N$_2$ mixtures. (a) $p = 1.0$ atm, $X_{N_2} < 0.004$. (b) $p = 1.2$ atm, $X_{N_2} = 0.007$. (c) $p = 1.2$ atm, $X_{N_2} = 0.015$. (d) $p = 2.8$ atm, $X_{N_2} = 0.035$.
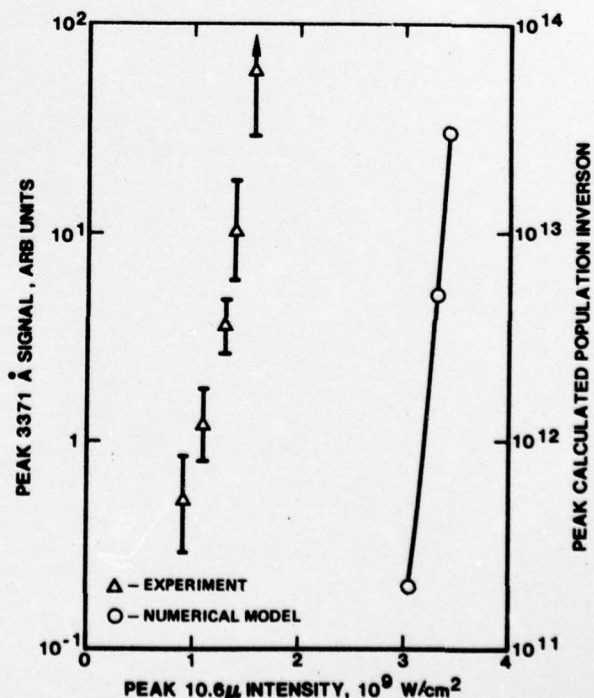

FIG. 4. Comparison between measured 3371-Å signal and calculated population inversion for various 10.6-μ peak intensities I_0. $p = 4.0$ atm, $X_{N_2} = 0.17$.

pumping intensity, characteristic of amplified spontaneous emission. The 3371-Å pulse shape and variation with I_0 will be discussed in Sec. III. The data in Figs. 3 and 4 clearly show the presence of laser action via amplified spontaneous emission. Because of the rather small size of the active discharge, the 3371-Å transition did not reach a saturated lasing condition in these experiments.

III. THEORETICAL STUDIES
A. Theoretical model

In order to gain insight into the kinetics of the optically pumped He/N_2 discharge, and to aid in interpreting the experimental data, a numerical simulation of the kinetic processes has been developed. This model is similar to that described in Refs. 10 and 11 for a conventional nitrogen laser. In the present model, processes involving quenching of the $C^3\pi_u$ and $B^3\pi_g$ levels by neutral molecules have been included, since these processes can be important at the high pressures of interest with the optically pumped discharge approach. The model assumes some initial value of electron density, and calculates the various discharge properties for a given 10.6-μ pulse shape and peak intensity. The processes considered in the model are listed in Table I, and the governing rate equations can be written as follows.

Ionization rate equation:

$$\frac{d[e]}{dt} = [e]k_7[N_2^X], \tag{1}$$

where $[e]$ is the electron density, $[N_2^X]$ is the nitrogen ground-state density, and k_7 is the rate coefficient associated with process (7) in Table I. Since we are interested in short-time scales (< 100 nsec), no loss processes have been included in the ionization rate equation. Also, for the range of electron energies and nitrogen fractions of interest here, the nitrogen dominates all of the inelastic processes. For the cases considered, process (8) was found to be negligible compared to process (7).

Excitation rate equations:

$$\frac{d[N_2^{C,0}]}{dt} = [e]k_5[N_2^X] - \frac{[N_2^{C,0}]}{\tau_C} - P, \tag{2}$$

$$\frac{d[N_2^{B,0}]}{dt} = [e]k_4[N_2^X] + \frac{[N_2^{C,0}]}{\tau_C} + P - \frac{[N_2^{B,0}]}{\tau_B}, \tag{3}$$

where

$$\tau_C = (k_{12} + [N_2^X]k_{14} + [He]k_{15} + [e]k_{16})^{-1},$$

$$\tau_B = (k_{13} + [N_2^X]k_{17} + [He]k_{18})^{-1}.$$

In these expressions, $[N_2^{C,0}]$ is the number density in the $C(^3\pi_u)_{v=0}$ state of nitrogen, $[N_2^{B,0}]$ is the density in the $B(^3\pi_g)_{v=0}$ state, P is the uv power density in photons/cm^3 sec, and the rates k_j refer to the processes in Table I. For the conditions of interest here, process (6) was negligible compared to process (5). Other processes, e.g., the reaction $e + N_2^{A,0} \rightarrow e + N_2^{C,0}$, were considered, and were found to be negligible for the conditions of interest here.

Electron energy equation:

$$\frac{e^2 I\nu}{m_e \epsilon_0 c(\omega^2 + \nu^2)} = (k_1\epsilon_1 + k_2\epsilon_2 + k_3\epsilon_3 + k_7\epsilon_7 + k_9\epsilon_9)[N_2^X]$$
$$+ [N_2^X]k_{10}\frac{3}{2}\frac{m_e}{m_{N_2}}(\bar{u}_e - \bar{u}_g)$$
$$+ [He]k_{11}\frac{3}{2}\frac{m_e}{m_{He}}(\bar{u}_e - \bar{u}_g), \tag{4}$$

where e is the electronic charge, I is the 10.6-μ intensity, ν is the momentum-transfer collision frequency, m_e is the electron mass, ϵ_0 is the free-space permittivity, c is the speed of light, ω is the laser angular frequency, $\bar{u}_e$ and $\bar{u}_g$ are the electron and gas temperatures, respectively, and the rates k_j and corresponding energies ϵ_j refer to Table I. In the electron energy equation, the rates of electronic excitation to all vibrational levels are included since they represent electronic energy losses, even though only excitations

TABLE I. Kinetic processes treated in the numerical model.

No.			Footnote
(1)	$e + N_2^X \rightarrow e + N_2^{A,0-20}$	Electronic excitation (multiple vibrational levels)	a
(2)	$e + N_2^X \rightarrow e + N_2^{B,0-18}$	Electronic excitation (multiple vibrational levels)	b
(3)	$e + N_2^X \rightarrow e + N_2^{C,0-4}$	Electronic excitation (multiple vibrational levels)	c
(4)	$e + N_2^X \rightarrow e + N_2^{B,0}$	Electronic excitation (ground vibrational level only)	d
(5)	$e + N_2^X \rightarrow e + N_2^{C,0}$	Electronic excitation (ground vibrational level only)	d
(6)	$e + N_2^{B,0} \rightarrow e + N_2^{C,0}$	Electronic excitation	e
(7)	$e + N_2^X \rightarrow e + e + N_2^+$	Ionization	f
(8)	$e + N_2^{C,0-4} \rightarrow e + e + N_2^+$	Ionization	e
(9)	$e + N_2^{X,0} \rightarrow e + N_2^{X,v}$	Vibrational excitation of the ground electronic state	f
(10)	$e + N_2^X \rightarrow e + N_2^X$	Momentum transfer	f
(11)	$e + He \rightarrow e + He$	Momentum transfer	f
(12)	$N_2^{C,0} \rightarrow N_2^{B,0} + h\nu$	Spontaneous decay	g
(13)	$N_2^{B,0} \rightarrow N_2^{A,0} + h\nu$	Spontaneous decay	g
(14)	$N_2 + N_2^{C,0} \rightarrow N_2 + N_2^{B,0}$	Quenching	g
(15)	$He + N_2^{C,0} \rightarrow He + N_2^{B,0}$	Quenching	h
(16)	$e + N_2^{C,0} \rightarrow e + N_2^{B,0}$	Quenching	e
(17)	$N_2 + N_2^{B,0} \rightarrow N_2 + N_2^{A,0}$	Quenching	g
(18)	$He + N_2^{B,0} \rightarrow He + N_2^{A,0}$	Quenching	h

^aCross section from Ref. 12 multiplied by $\frac{1}{3}$ based on discussion in Ref. 12 and in order to bring the value into closer agreement with that in Ref. 14.
^bCross section from Ref. 12.
^cCross section from Ref. 12 multiplied by 1/1.5 based on same arguments as footnote a.
^dCross section obtained from multiple-vibrational-level cross section by multiplying by appropriate Frank-Condon factor.
^eRate from Ref. 11.
^fCross section from Ref. 13.
^gRate from Ref. 15.
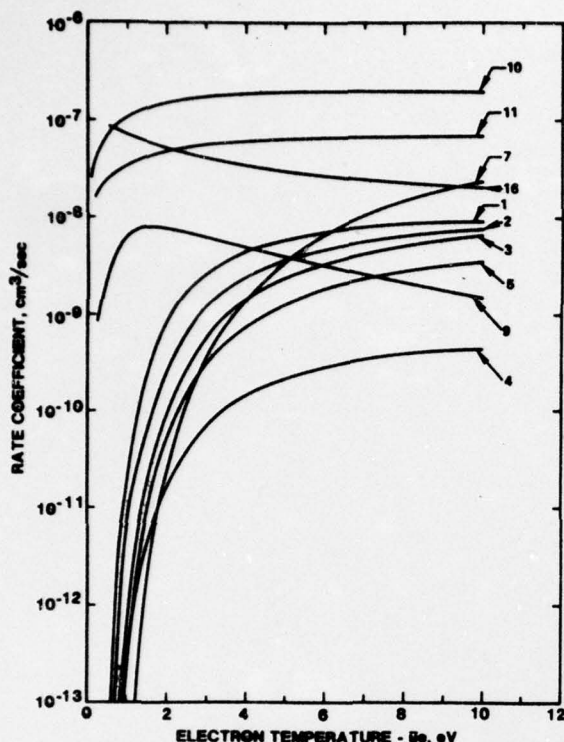^hRate estimated based on Ref. 15.

FIG. 5. Rate coefficients used in the numerical model. (Numbers correspond to Table I.)

FIG. 6. Calculated inversion densities and electron densities for various 10.6-μ peak intensities. $p = 4.0$ atm, $X_{N_2} = 0.17$. (For comparison, the 10.6-μ pulse shape is also shown).

to the ground vibrational levels are of importance in determining the population inversion.

In addition to the above equations, the vibrational temperature $\bar{u}_v$ and gas temperature $\bar{u}_e \equiv \frac{3}{2}kT_e$ were calculated from the appropriate equations. These quantities were used primarily to check for depletion of the ground level due to electron excitation or to thermal excitation.

The various processes, along with the sources of the various rate data are shown in Table I. The electron impact rates are plotted in Fig. 5. These rates were obtained by integrating the appropriate cross sections over a Maxwellian energy distribution function. The Cartwright cross section[12] for the $X^1\Sigma_g^+ \rightarrow A^3\Sigma_u^+$ process was multiplied by the factor $\frac{1}{3}$, based on the discussion in Ref. 12, and in order to bring the value into better agreement with the value presented in Ref. 14. For the same reasons, the cross section for the $X^1\Sigma_g^+ \rightarrow C^3\pi_u$ process was multiplied by the factor 1/1.5.

In addition to the above rate equations, the 10.6-μ absorption length l_a was calculated from the expression

$$l_a = \frac{m_e \epsilon_0 c (\omega^2 + \nu^2)}{[e] e^2 \nu} . \tag{5}$$

B. Comparison of theory with experiment

As mentioned in Sec. II, the experimental data were obtained under conditions in which the uv laser transition was not saturated. In order to compare the theoretical model with these data, calculations were carried out as follows. The uv power density P in Eqs.
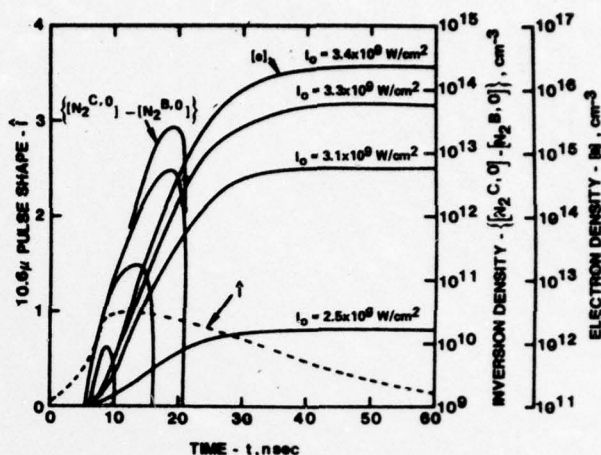
(2) and (3) was set equal to zero, giving three equations for the unknowns $[e]$, $[N_2^{C,0}]$, and $[N_2^{B,0}]$, with Eq. (4) giving $\bar{u}_e$ for each value of I. Typical results are shown in Fig. 6, in which a 10.6-μ pulse shape approximating that in the experiments has been used, and where an initial electron density of 10^{11} cm^{-3} was assumed. The plots show the electron density and the inversion density vs time during the pumping pulse.

It should be pointed out that in the calculation, the 10.6-μ intensity was assumed to be uniform over the volume under consideration; whereas, in the experiment, the 10.6-μ intensity varied spatially due to the transverse beam profile and due to the attenuation by the discharge. Thus, the calculation represents points near the centerline of the focal volume and is strictly valid only for conditions in which the absorption length l_a is comparable to or greater than the focal volume length. For all of the curves in Fig. 6, the calculated absorption length was in excess of 50 cm (i.e., long compared to the 10-cm focal volume length) during the time in which an inversion existed.

Two trends are apparent from the curves in Fig. 6. First, the peak inversion occurred near the peak of the 10.6-μ pulse, and the inversion had a time duration of approximately 10 nsec, as would a pulse of amplified-spontaneous-emission radiation corresponding to this inversion. This trend is in qualitative agreement with the detector traces in Fig. 3. For these conditions, the decay time τ_C had a value of approximately 3 nsec, and as seen from Fig. 6 once the 10.6-μ intensity (and the electron temperature) began to fall, the inversion decayed on this same time scale.

A second trend seen in Fig. 6 is the strong dependence of the peak inversion density and of the electron density on the 10.6-μ intensity. While the experimental variation of electron density with I_0 was not quite as rapid as indicated in Fig. 6, the dependence on I_0 was still strong, as indicated in Figs. 2(c) and 2(d). This effect required a high level of pulse-to-pulse repeatability in the TEA pumping laser in order to obtain reliable results with optical discharge pumping. In Fig. 4, the

peak inversion densities, obtained from Fig. 6, are plotted for comparison with the peak uv signals. The inversion density (rather than the exponential of the inversion density) is probably a good comparison, since in the experiments the intense portion of the discharge (i.e., the effective gain length) appeared to decrease as the pumping intensity was increased. It can be seen that the two curves in Fig. 4 do show reasonably good agreement.

C. Coupling and efficiency calculations

In any practical laser utilizing the optically pumped discharge concept, conditions would be chosen such that the uv radiation field would saturate the $C^3\pi_u \to B^3\pi_g$ transition (either through use of a uv optical cavity or by making the system large enough so that the amplified-spontaneous-emission intensity reached saturation[16]). The section describes results obtained modeling the latter condition. As discussed in Refs. 10 and 11, when the transition is saturated ($[N_2^{C,0}] \approx [N_2^{B,0}]$), Eqs. (2) and (3) can be rewritten

$$\frac{d[N_2^{C,0}]}{dt} = \tfrac{1}{2}([e][N_2^X][k_4 + k_5]) - \frac{[N_2^{C,0}]}{2\tau_B} \qquad (6)$$

and

$$P = \tfrac{1}{2}\left([e][N_2^X][k_5 - k_4] - \frac{2 - (\tau_C/\tau_B)}{\tau_C}[N_2^{C,0}]\right). \qquad (7)$$

In modeling large-scale laser systems, the uv flux was treated in two ways. During the initial buildup of the electron density, the transition was assumed to be unsaturated, and the inversion was calculated using Eqs. (2) and (3) with $P = 0$. When the total gain reached 30 dB (using a cross section for stimulated emission of 10^{-15} cm^2), the transition was assumed to be saturated and the uv power was calculated using Eq. (7). This approach was qualitatively useful in determining the onset of lasing, and should give accurate quantitative results for conditions well above threshold.

The purpose of the saturated-power calculation was to investigate the energy-transfer processes in the discharge and to examine the parameters which determine the efficiency of conversion from 10.6-μ radiation to 3371-Å radiation. In doing this, it was useful to define two efficiency factors. The coupling efficiency η_C can be defined as

$$\eta_C \equiv \frac{\text{power coupled into uv field}}{\text{power absorbed from 10.6-}\mu\text{ field}},$$

and can be written

$$\eta_C = \frac{P\epsilon_\bullet}{I_{10.6}/l_d}, \qquad (8)$$

where $\epsilon_\bullet$ is the photon energy. A total efficiency η_T can be defined as

$$\eta_T \equiv \frac{\text{uv energy coupled out of the discharge}}{\text{10.6-}\mu\text{ energy incident on the discharge}},$$

and can be written

$$\eta_T = (l_d \int_0^T P\epsilon_\bullet \, dt)(\int_0^T I \, dt)^{-1}, \qquad (9)$$

where l_d is the discharge length and T is the 10.6-μ pulse length. (In this expression, it is assumed that the 10.6-μ focal volume and the uv laser axis are coaxial).

The quantity η_C can be interpreted as a microscopic efficiency and is a measure of the effectiveness with which the energy deposited in the electrons is converted into uv photons. The coupling efficiency can in turn be written as the product of three factors as

$$\eta_C = \eta_{EC}\eta_{CB}\eta_Q,$$

where η_{EC} is the fraction of energy deposited in the electrons which channels into the upper laser level, η_{CB} is the fraction of energy in the upper level which goes into stimulated emission, rather than into spontaneous emission or quenching, and η_Q is the quantum efficiency ($\eta_Q = \epsilon_\bullet/\epsilon_5$).

The factor η_{EC} can be examined directly by looking at Eq. (4). For most cases of interest, the elastic losses are negligible compared to the inelastic losses, and η_{EC} can be written

$$\eta_{EC} \approx k_5\epsilon_5/\sum_j k_j\epsilon_j,$$

where the summation is over the inelastic terms on the right-hand side of Eq. (4). This quantity, which is a function only of the electron temperature, is plotted in Fig. 7. It can be seen that in order to keep this factor high, it is necessary to maintain $\bar{u}_e$ above 4 eV. A similar result was obtained in Ref. 11.

The factor η_{CB} can be examined by looking at Eq. (7). The factor of $\tfrac{1}{2}$ can be interpreted physically as follows. Since the transition is bottlenecked ($\tau_C \ll \tau_B$), the inversion can only be maintained on a transient basis and each stimulated emission event reduces the inversion by two molecules. Thus, even under conditions where
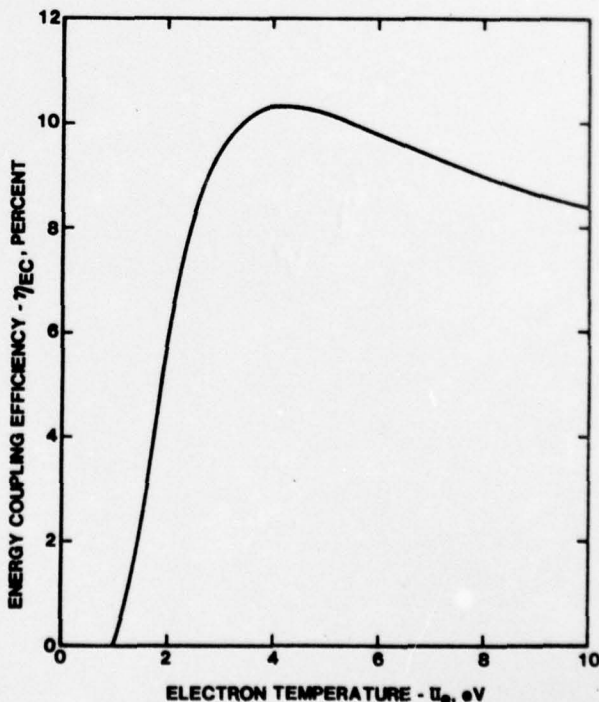

FIG. 7. Energy coupling efficiency vs electron energy.

stimulated emission dominates spontaneous emission and quenching, the factor η_{CB} is limited to a value of $\frac{1}{2}$.

Based on these arguments, the upper limit on the value of η_C for the 3371-Å nitrogen transition ($\eta_Q = 0.33$) is $(\eta_C)_{max} \approx (0.10)(0.5)(0.33) = 0.016 = 1.6\%$. This result depends only on the collisional rates, and is independent of the method of electron heating (i. e., dc discharge, rf discharge, electron beam, or optically pumped discharge).

In developing a working laser, one cannot maintain η_C at its optimum value during the entire pumping pulse because of temporal and spatial variations in η_{EC} (through variations in $\bar{u}_e$) and in η_{CB} (due to such things as quenching and laser threshold effects). Thus, once one has selected a kinetic system with a reasonably high value of $(\eta_C)_{max}$, the problem of optimizing the laser design becomes one of developing a pumping scheme which can maintain this value of η_C over the entire active volume and during a significant fraction of the pumping pulse.

This problem is very difficult in the nitrogen system because of the coupling between the laser kinetics and the ionization kinetics. As mentioned above, it is desirable to maintain $\bar{u}_e$ above 4 eV. However, as seen from Fig. 5, for a nitrogen pressure of 50 Torr and $\bar{u}_e = 4$ eV, the ionization time $\tau_I = ([N_2^X]k_7)^{-1}$ is 0.5 nsec. Thus, the electron density builds up very quickly under optimum laser-pumping conditions. In the dc discharge this results in a mismatch between the discharge impedance and the driving circuit with a corresponding drop in $\bar{u}_e$ and with a large fraction of the stored electrical energy being dissipated in the external circuit rather than in the discharge.

In the case of the optically pumped discharge, the value of $\bar{u}_e$ can be maintained at a high value even for large values of $[e]$ [see Eq. (4)]. However, if $\bar{u}_e$ is maintained at a high value for too long a period of time, the ionization process will go all the way to breakdown (see Fig. 2). Thus for both dc and optical pumping, the ionization process favors short pumping pulses, and tends to be an even more stringent constraint than laser bottlenecking. [10]
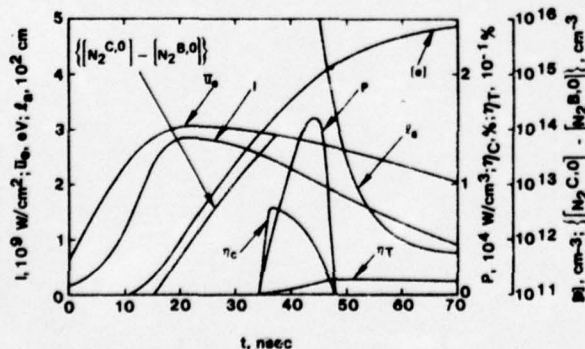
Typical numerical results, illustrating some of these effects are shown in Figs. 8 and 9. In Fig. 8, a 10.6-μ pulse shape typical of that in the experiments was used. The onset of uv saturation was based on an active length of 100 cm, and the peak value of I was chosen so that l_a stayed above a value of 75 cm during the pulse. With these constraints, the coupling efficiency varied from $\sim 0.8\%$ at the beginning of the uv pulse to $\sim 0.5\%$ at the peak of the uv pulse. The corresponding total efficiency reached a peak value of $\sim 0.01\%$. The rapid cutoff of the uv pulse was caused by electron quenching.

The case shown in Fig. 9 represents a better match between the pumping pulse and the discharge kinetics. The nitrogen and helium densities were chosen so that their quenching rates were equal to the spontaneous emission rate from the $C^3\pi_u$ level. The 10.6-μ peak intensity and pulse shape were chosen so that $\bar{u}_e$ remained high during the uv pulse, but so that $[e]$ remained low enough to reduce quenching of the $C^3\pi_u$ level. These conditions corresponded to $l_a)_{min} = 230$ cm and a value $l_d = 500$ cm was used. This result shows that for this kinetic system, the optical pumping approach becomes more favorable for very large laser systems.

The value of $\bar{u}_e$ for these conditions was higher than in Fig. 8, and η_C varied from 1.2% at the beginning of the uv pulse to 0.9% at the peak of the pulse. The corresponding total efficiency was 0.35%. The gas temperature reached a value of 307°K, and the vibrational temperature was 700°K at the end of the uv pulse, indicating that vibrational depopulation of the ground state would not be a problem. The results in Fig. 9 show that the electron temperature follows the 10.6-μ intensity directly, and that the coupling efficiency follows $\bar{u}_e$ during the time when the uv laser transition is saturated. The factor-of-30 improvement in η_T from Fig. 8 to Fig. 9 resulted from the higher electron temperature during the uv pulse, from the better overlap between the uv pulse and the 10.6-μ pulse, and from the reduction of electron quenching of the upper laser level.

While Fig. 9 probably does not represent the optimum conditions it does illustrate the approach that can be used in seeking the optimum set of parameters (e.g.,

FIG. 8. Calculated discharge properties vs time. $p = 0.4$ atm, $X_{N_2} = 0.10$, $l_d = 1.0 \times 10^2$ cm. The symbols used are as follows: t—time, I—10.6-μ intensity, $\bar{u}_e$—electron energy, l_a—10.6-μ absorption length, P—uv power density, η_C—coupling efficiency, η_T—total efficiency, $[e]$—electron density, $([N_2^{C,0}] - [N_2^{B,0}])$—inversion density.
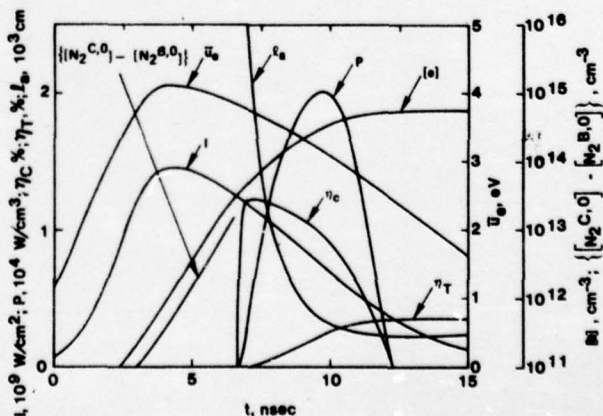

FIG. 9. Calculated discharge properties vs time. $p = 2.0$ atm, $X_{N_2} = 0.02$, $l_d = 5.0 \times 10^2$ cm. The symbols used are the same as in Fig. 8.

pressure, nitrogen fraction, 10.6-μ pulse shape, 10.6-μ pulse length, discharge length, etc.). The peak value of η_c in Fig. 9 is close to the maximum value estimated above from simple energy channeling considerations and the total efficiency of 0.35% is within a factor of 4 of the maximum coupling efficiency. With further optimization, a total efficiency of 1% could probably be achieved. Since TEA lasers operating with pulses of the approximate shape shown in Fig. 9 could be expected to have an efficiency of 10%, the total efficiency of this system (stored electrical energy to uv laser energy) is probably limited to a value of 0.1–0.2%. While this value is comparable to values attainable with conventional large-volume nitrogen lasers,[17] it is somewhat marginal for most large-scale uv laser applications. For this reason, the optically pumped discharge approach is probably of greater interest when applied to other kinetic systems.[2-4]

IV. SUMMARY AND CONCLUSIONS

Experimental studies have shown that the optically pumped discharge technique is capable of generating high-density diffuse discharges at pressures up to 12 atm. Measurements of the 3371-Å radiation from a helium-nitrogen mixture at 4.0 atm showed the presence of amplified spontaneous emission along the axis of the discharge.

An analytical model of the discharge kinetics showed variations in the electron density and small-signal gain which were in qualitative agreement with the experimental results. This analytical model was used to study the coupling and efficiency effects in the discharge and it was shown that the total efficiency of conversion from 10.6-μ energy to uv laser energy is determined by the microscopic kinetic transfer efficiency and by the ability of the pumping technique to maintain the optimum microscopic efficiency over a large fraction of the active volume and during a large fraction of the pumping pulse. Because of the rather low microscopic efficiency inherent in direct electron-impact pumping of the nitrogen 3371-Å transition, and because of limitations due to the discharge dynamics, the optically pumped helium-nitrogen system studied here does not appear promising as a high-efficiency high-energy uv laser. However, many of the concepts discussed in this study are applicable to other kinetic systems which do have higher potential efficiencies.

[1]B. Godard, IEEE J. Quantum Electron. QE-10, 147 (1974).
[2]H.A. Koehler; L.H. Ferderber, D.L. Redhead, and P.J. Ebert, Appl. Phys. Lett. 21, 198 (1972).
[3]E.R. Ault, M.L. Bhaumik, and N.T. Olson, IEEE J. Quantum Electron. QE-10, 624 (1974).
[4]C.B. Collins, A.J. Cunningham, and M. Stockton, Appl. Phys. Lett. 25, 344 (1974).
[5]R.T. Brown and D.C. Smith, Appl. Phys. Lett. 24, 236 (1974).
[6]R.T. Brown and D.C. Smith, Appl. Phys. Lett. 22, 245 (1973).
[7]The beam profile was approximately Gaussian, and the experimental values of 10.6-μ intensity refer to the centerline intensity.
[8]D.C. Smith and R.T. Brown, J. Appl. Phys. 46, 1146 (1975).
[9]R.W. Waynant, Laser Focus 9, 41 (1973).
[10]E.T. Gerry, Appl. Phys. Lett. 7, 6 (1965).
[11]A.W. Ali, A.C. Kolb, and A.D. Anderson, Appl. Opt. 6, 2115 (1967).
[12]D.C. Cartwright, Phys. Rev. A 2, 1331 (1970).
[13]E.W. McDaniel, *Collision Phenomena in Ionized Gases* (Wiley, New York, 1964).
[14]A.G. Engelhardt, A.V. Phelps, and C.G. Risk, Phys. Rev. A 135, 1566 (1964).
[15]R.M. Hill, R.A. Gutcheck, D.L. Huestis, D. Mukherjee, and D.C. Lorentz, SRI Report No. MP74-39, 1974 (unpublished).
[16]D.A. Leonard, Appl. Phys. Lett. 7, 4 (1965).
[17]V. Hasson, D. Preussler, J. Klimek, and H.M. von Bergmann, Appl. Phys. Lett. 25, 654 (1974).

DISTRIBUTION

Director   2
Advanced Research Projects Agency
1400 Wilson Boulevard
Arlington, VA   22209

Defense Documentation Center   12
Cameron Station
Alexandria, VA   22314

Office of Naval Research   3
800 North Quincy Street
Arlington, VA   22217
Attn: Code 421

Director   12
Naval Research Laboratory
Washington, D. C.   20375
Attn: Code 2629
Attn: Code 2627

Office of Naval Research
495 Summer Street   1
Boston, MA   02210

Naval Plant Representative Office   1
Pratt & Whitney Aircraft
East Hartford, CT   06108